minerals

MDPI

Article

Fluid Evolution of Greisens from Krupka Sn-W Ore District, Bohemian Massif (Czech Republic)

Michaela Krejčí Kotlánová [1,2,3], Zdeněk Dolníček [4,*], Miloš René [5], Walter Prochaska [6], Jana Ulmanová [4], Jaroslav Kapusta [7], Vlastimil Mašek [†] and Kamil Kropáč [7]

[1] Department of Geological Sciences, Masaryk University, Kotlářská 267/2, 611 37 Brno, Czech Republic; kotlmi@seznam.cz
[2] Research Institute for Building Materials, Hněvkovského 30/65, 617 00 Brno, Czech Republic
[3] BIC Brno Spol. s r.o., Technology Innovation Transfer Chamber, Purkyňova 648/125, 612 00 Brno, Czech Republic
[4] Department of Mineralogy and Petrology, National Museum, Cirkusová 1740, 193 00 Praha, Czech Republic; jana.ulmanova@nm.cz
[5] Institute of Rock Structure and Mechanics, Academy of Sciences of the Czech Republic, V Holešovičkách 94/41, 182 09 Praha, Czech Republic; rene@irsm.cas.cz
[6] Österreichisches Archäologisches Institut, Franz Klein-Gasse 1, 1190 Wien, Austria; walter.prochaska@oeaw.ac.at
[7] Department of Geology, Palacký University, 17. Listopadu 1192/12, 771 46 Olomouc, Czech Republic; jaroslav.kapusta@upol.cz (J.K.); kamil.kropac@upol.cz (K.K.)
* Correspondence: zdenek.dolnicek@nm.cz
† Deceased author.

Abstract: The Sn-W ore deposits in the Krupka surroundings are associated with greisens, which occur in the upper parts of Late Variscan granitoid intrusions. Fluid inclusions were studied in samples of quartz, cassiterite, apatite, fluorite, and topaz in greisenized granites, greisens, and hydrothermal veins with Sn-W mineralization. The greisenization process took place at temperatures 370–490 °C and pressures 155–371 bars, and associated fluids had predominantly low salinity and a low gas (CO_2, N_2 and CH_4) content. The post-greisenization stage was connected with the formation of (i) low-salinity (0–8 wt. % NaCl eq.) fluid inclusions with homogenization temperatures <120–295 °C and (ii) high-salinity (18 to >35 wt. % NaCl eq.) fluid inclusions with homogenization temperatures 140–370 °C, often containing trapped crystals of quartz, topaz, and sulfides, or daughter crystals of salts and carbonates, which were identified by microthermometric measurements, electron microprobe analysis, and Raman spectroscopy. Analyses of fluid inclusion leachates have shown that Na and Ca chlorides predominate in fluids. According to hydrogen stable isotopes, the source of greisenizing and post-greisenizing fluids was not only magmatogenic but also meteoric water or fluids derived from sedimentary rocks.

Keywords: Krupka; Bohemian Massif; greisen; Sn-W mineralization; fluid inclusions; stable isotopes of hydrogen; crush-leach analyses; Raman spectroscopy

check for updates

Citation: Krejčí Kotlánová, M.; Dolníček, Z.; René, M.; Prochaska, W.; Ulmanová, J.; Kapusta, J.; Mašek, V.; Kropáč, K. Fluid Evolution of Greisens from Krupka Sn-W Ore District, Bohemian Massif (Czech Republic). *Minerals* **2024**, *14*, 86. https://doi.org/10.3390/min14010086

Academic Editors: Yuichi Morishita and Napoleon Q. Hammond

Received: 19 December 2023
Revised: 3 January 2024
Accepted: 8 January 2024
Published: 11 January 2024

Copyright: © 2024 by the authors. Licensee MDPI, Basel, Switzerland. This article is an open access article distributed under the terms and conditions of the Creative Commons Attribution (CC BY) license (https://creativecommons.org/licenses/by/4.0/).

1. Introduction

The Erzgebirge/Krušné hory mountains are rich in occurrences of Sn-W mineralization bound to greisens, which form the apical parts of Late Variscan granitoid intrusions. In the western part of the Saxothuringian Zone of the Bohemian Massif, these occurrences are more abundant and are represented by deposits in Krásno near Horní Slavkov, in Přebuz, Rolava, and Podlesí in the Blatná granite body. In the east, the most important localities, where tin and tungsten ores were historically mined, are Krupka and Cínovec.

Older (OIC) and younger intrusive complex (YIC), differing in age and rock chemistry, were distinguished in the Krušné hory/Erzgebirge Batholith [1]. Opinions on the formation of highly fractionated granites and associated greisens are evolving, and there

are many supporters of both magmatic and metasomatic origins of fluids that form these rocks. [2] assumed that all YIC granites were formed by the hydrothermal transformation of granites belonging to OIC granites. The mentioned author developed the theory of autometamorphism, which explains the transformation of granites in the postmagmatic stage due to the activity of cogenetic hydrothermal solutions. Ref. [3] considered the zonal structure of the YIC granites, the theory of albitization, and other metasomatic processes. Many authors are inclined toward the metasomatic origin of fluids that can form YIC granites, e.g., [4,5].

An often-accepted theory of the formation of highly fractionated granites involves their primary magmatic origin, where enrichment in volatile components and incompatible elements occurs during fractional crystallization [6]. When the magma rises to the surface, gradually smaller volumes of more differentiated melts are enriched in incompatible components (Rb, Cs, Li and others), including H_2O and other volatile substances (F, B), eventually leading to their segregation [7]. Another clue that supports a magmatogenic origin of fluids is the finding of magmatic breccias at several localities, e.g., Krupka, Horní Slavkov, and Podlesí. These rocks are formed by fragments of gneisses or phyllites cemented by granite matrix [8–11]. Many authors accept the opinion that greisenization fluids have a magmatogenic origin—e.g., [12,13].

The research of stable isotopes of hydrogen and oxygen in altered (greisenized) granites from the locality Cínovec and Krásno-Hub Stock [14] showed that the origin of greisenizing fluids is not only magmatogenic but partly also in meteoric waters and fluids derived from sedimentary rocks.

From a mineralogical and petrological point of view, the greisens in the Czech part of the Krušné hory/Erzgebirge Mts. are relatively well described, but comprehensive information about the genesis and formation conditions of greisens is lacking. Investigations of fluid inclusions in the minerals of greisens from the Czech part of the Saxothuringian Zone of the Bohemian Massif were mainly carried out by [15–18]. A large amount of data on the topic of fluid inclusions in greisens and associated hydrothermal veins from the Krupka ore district was collected by [15]. The aim of this research was to collect new data on temperature and pressure conditions of the formation of greisens and associated hydrothermal veins and try to determine the origin and composition of greisenizing and younger fluids at the Krupka ore district. This article expands the topic with new knowledge obtained by modern research methods.

2. Geological Settings

2.1. The Krušné Hory/Erzgebirge Crystalline Complex

The Krušné hory/Erzgebirge Crystalline Complex occurs in the northwestern part of the Bohemian Massif and is formed by a diverse sequence of metamorphic rocks of various protolith ages ranging from the Precambrian to the Lower Paleozoic. The intensity of Variscan metamorphosis decreases to the northwest. In the northeast, the rocks are represented by Proterozoic paragneisses, and in the southwest, by Ordovician phyllites and quartzites. The central part of the Saxothuringian unit is formed by Cambrian mica schists. In the north and northwest, Saxothuringian units sink beneath Permo-Carboniferous, Mesozoic, Tertiary, and Quaternary sediments [19,20]. Crystalline units are intruded by granitic plutons of the Variscan age (Figure 1).

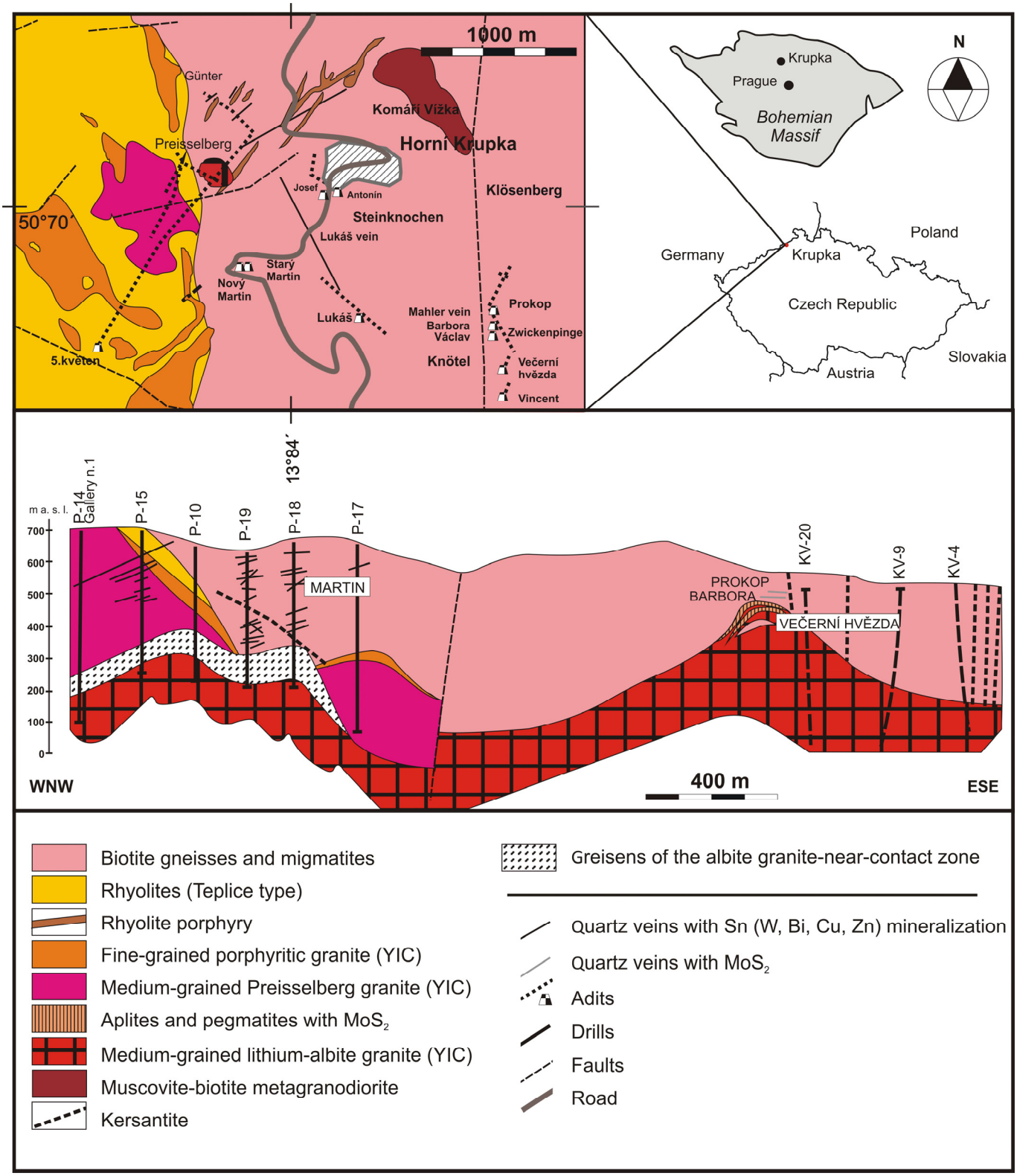


Figure 1. Geological map of the Krupka ore district with the location of the main ore fields and abandoned mine workings (modified after [21]) and the WNW–ESE geological cross-section through the Krupka surroundings (modified after [22]).

2.2. Krušné Hory/Erzgebirge Batholith

The Krušné hory/Erzgebirge Batholith was considered by the first geologists to be a single body [23,24], but it was later found that in space and time, there are several intrusions

with their own evolution and different ages [25,26]. The Karlovy Vary, Nejdek-Eibenstock, Kirchberg, and Bergen plutons are described in the west of the Saxothuringian Zone of the Bohemian Massif. From the central part, the Geyer granite body, the Hora Svaté Kateřiny, and Hora Svatého Šebestiána bodies are known. In the east, the Telnice granite body and the Altenberg caldera occur [26–28].

As mentioned in the introduction, two types of granites were distinguished within the Krušné hory/Erzgebirge Batholith, differing in their age and chemical composition. The low-F granites of OIC included porphyritic biotite granites, granodiorites, and granites. The high-F granites of YIC were represented by coarse-grained, sometimes porphyritic, muscovite-biotite or tourmaline-biotite granites and Li-mica granites, which are Si-rich, reduced, and strongly peraluminous and are often affected by processes of autometamorphism and have increased contents of incompatible elements [1]. The Li-mica granites have crustal isotopic signatures [26]. The transitional types are sometimes present between OIC and YIC. According to chemistry, two subtypes of OIC and YIC granites—weakly and strongly peraluminous—are further distinguished [25]. Strongly peraluminous granites correspond to S-type granites, are enriched in P, and have relatively low content of HFSE and HREE. The weakly peraluminous granites correspond to A- and I-type granites and have a very low content of P and increased amounts of HFSE and HREE. The granites in the Krupka ore district belong to the younger generation of slightly peraluminous P-poor granites [25]. Compared to the rest of European Variscides, the Krušné hory/Erzgebirge Batholith exhibits a relatively high abundance of Li-mica granites. However, the reason is still not completely resolved because the isotopic composition of Li-mica granites does not differ significantly from peraluminous granites from other regions. However, the underlying gneisses and metasediments have high contents of incompatible elements, and this can also be an explanation for the different composition of granites in the Krušné hory/Erzgebige Batholith [26]. Granites of OIC are of the Upper Viséan–Westphalian age (340 Ma to 310 Ma) [20,29]. The age of the granites of YIC was estimated at 285 to 329 Ma [30–33]. Granites of YIC are often affected by greisenization [13,17,18] and connected with economically important accumulations of Sn, W, and Li.

2.3. Geological Situation of the Krupka Ore District

The geological situation in the Krupka ore district is relatively complicated. Two geological units meet there: (i) the gneiss complex, composed of Freiberg orthogneisses in the east and in the west with biotite paragneisses, and (ii) the Teplice rhyolite complex with different porphyritic rocks. The Teplice rhyolite complex is, in places, crosscut by granite porphyries and intruded by the granites of the younger intrusive complex (see Figure 1).

There are three ore deposits around Krupka town surroundings—Preisselberg, Knötel, and Komáří Vížka. The Preisselberg body consists mainly of fine-grained porphyritic biotite granite. In the central part, a drill hole reached lithium albitized apogranite with quartz-topaz-(zinnwaldite) greisen in its apical part. Two stages of greisenization are described here. The older one is connected with the formation of dark W-bearing mica-quartz greisen, whereas the younger one resulted in the formation of quartz-topaz-mica greisen. Ore mineralization consists of wolframite, cassiterite, scheelite, and sulfides. In the northeast, there is present an important hydrothermal vein, Lukáš, with a thickness of up to 0.5 m and abundant Sn-W mineralization. In the vicinity of the vein, the greisenization of rocks connected with the formation of Li-Fe micas and topaz is evident. The marginal parts of the Preisselberg granite are lined with pegmatite, composed mainly of quartz and K-feldspar [22]. At Komáří Vížka, gneisses are intersected by felsic quartz porphyries affected by greisenization. Greisens are quartz-Li-mica-topaz rocks with cassiterite and abundant amounts of sulfides. The Knötel deposit is the largest district in this area and is located in the north of Krupka. Under the mantle gneisses, which are sometimes crosscut by aplite veins and composed of quartz, topaz, micas, and feldspars, hidden bodies of lithium apogranite have been found by drill holes [34]. These rocks are greisenized in places. At Prokop Stock, which forms the apical part of the granite body, there is an

occurrence of quartz greisen and quartz veins with abundant molybdenite and fluorite in the top parts of the body. Refs. [35,36] refer to these light rocks as quartz greisens, hydrothermal quartzites, or quartzite-like rocks. These rocks are formed mainly by quartz in association with molybdenite, fluorite, and accessory topaz, mica, clay, and ore minerals. The above-mentioned authors describe nests/pockets of massive quartz with molybdenite. Quartzite-like rocks contain gneiss xenoliths or form the matrix of breccias with fragments of surrounding gneisses and pegmatites. The lower parts of the body are formed by pegmatite, which was encountered by the adits Barbora and Večerní hvězda and consists mainly of K-feldspar, coarse-grained quartz, and biotite. Pegmatite is crosscut by aplite veins, quartz veins, and vein-type (crack-type) greisens. The mineral composition of greisens ranges from zinnwaldite-quartz greisen to light gray quartz greisen with topaz [22]. Ref. [37] distinguished four stages of the formation of ore mineralization in the Krupka ore district—albitization, greisenization, the formation of sulfides, and the formation of fluorite and carbonates.

3. Materials and Methods

Some samples for the study were collected from dump material occurring in the Krupka ore district. Another part of the samples was borrowed from the collections of the National Museum in Prague and Mgr. Jakub Mysliveček from Czech Geological Survey.

The doubly polished thin sections were prepared for the study of the fluid inclusions in quartz, topaz, cassiterite, fluorite, and apatite. The sections were examined using a polarizing microscope in reflected light and subsequently also in backscattered electrons (BSE) on electron microprobe Cameca SX-100 (AMETEK, Inc., Berwyn, PA, USA) in the National Museum in Prague.

Petrography of fluid inclusions was studied using polarizing microscopes Olympus BX50 (Olympus Co., Tokyo, Japan) and Nikon Eclipse LV100ND (Nikon Co., Tokyo, Japan). Then, microthermometry of fluid inclusions was performed using an Olympus BX51 microscope equipped with a Linkam THMSG 600 heating-freezing microthermometric chamber (Linkam Scientific Instruments, Surrey, UK) at the Department of Geology, Palacký University in Olomouc, Czech Republic. Primary, pseudosecondary, and secondary inclusions were studied in order to characterize all stages of fluid evolution associated with Sn-W mineralization, greisenization, and post-greisenization stages. The following parameters were measured: freezing temperature (Tf), melting temperature of the last crystal of ice (Tm_{ice}), homogenization temperature to vapor (Th_V), homogenization temperature to liquid (Th_L), homogenization temperature critical (Th_C), eutectic temperature (Te), clathrate melting temperature (Tm_{cla}), and dissolution temperature of halite (Tds_h). The measurement was calibrated between −56.6 and 374.1 °C with inorganic standards and natural fluid inclusions with known temperatures of phase transitions. The reproducibility of measurement is within 0.1 °C for temperatures between −56.6 and 0 °C, and within 1 °C for temperature of 374.1 °C.

The salinity of inclusions enclosing the H_2O-NaCl system (with Tm_{ice} from 0 to −21.3 °C) was calculated according to [38]. The composition, density, and molar volume of volatile gas-bearing FI were calculated using the programs ICE and BULK according to [39,40]. For fluid inclusions trapped from a heterogeneous fluid, the bulk density and composition of the inclusions were calculated in the BULK program according to [41], and then the pressure conditions of inclusion entrapment were calculated in the ISOC program according to [42,43] for H_2O-CO_2-NaCl fluids and [44,45] for H_2O-NaCl fluids. Programs ICE, BULK, and ISOC are included in the FLUIDS 1 and FLUIDS 2 program packages, available on the website of the University of Leoben [46].

Fluid inclusion leachates were analyzed in selected samples of quartz from greisens and veins. Samples were first crushed to a fraction of 0.3–1.1 mm and subsequently boiled in distilled water. Thereafter, the samples were dried, and other mineral phases and impurities were handpicked under a binocular microscope. A weighed quantity of quartz (1 g) was washed in deionized water and subsequently dried at 50 °C. One gram of the dried sample was ground

in an agate mortar together with 5 mL of deionized water. Subsequently, the suspension was filtered through a 0.2 μm nylon filter. Analysis of the filtrate was performed using an ion chromatograph Dionex DX-500 (Thermo Fisher Scientific, Inc., Waltham, MA, USA). Detection limits are as follows: Cl (10 ppb), Br (2 ppb), F (5 ppb), I (0.1 ppb), and SO_4 (10 ppb).

In selected samples, Raman analysis was used to identify volatiles and solid phases enclosed in fluid inclusions. The analyses were carried out at the Institute of Molecular and Translational Medicine, Faculty of Medicine, Palacký University, Olomouc (Czech Republic). The samples were examined on the WITec Confocal Raman Imaging Microscope System alpha300 R+ spectrometer (Oxford Instruments, Abingdon, Oxfordshire, UK) with an excitation of 532 nm (25 mW power incident on the sample, lens 50×/NA 0.8, spectrum acquisition time 1 min). Part of the Raman analysis was carried out at the National Museum in Prague (Czech Republic) on the DXR dispersive Raman Spectrometer (Thermo Fisher Scientific, Inc., Waltham, MA, USA) mounted on a confocal Olympus microscope. The Raman spectra were collected in the range 4000–30 cm^{-1}; however, for our purposes, the unnecessary part of the spectrum was subsequently cut off. The instrument was set up by a software-controlled calibration procedure using multiple neon emission lines (wavelength calibration), multiple polystyrene Raman bands (laser-frequency calibration) and standardized white-light sources (intensity calibration). The Raman signal was excited by an unpolarized green 532 nm solid state, diode-pumped laser, and detected by a CCD detector. The experimental parameters: 100× objective, 5 s exposure time, 100 exposure, 50 μm pin spectrograph aperture, and 10 mW laser power level. The spectra were repeatedly acquired from different places/focus depths in order to obtain a representative spectrum with the best signal-to-noise ratio. The eventual thermal damage of the measured point on solid phases was excluded by visual inspection of the excited surface after measurement, by observation of possible decay of spectral features at the start of excitation and by checking for thermal downshift of Raman lines. Spectral manipulations were performed using the Omnic 9 software (Thermo Scientific). Publications of [47,48] were used for the determination of individual gaseous components, and the identification of solid phases was carried out according to the data contained in [49]. The quantification of gases in the non-aqueous phase of fluid inclusions was based on the measurement of peak areas [47] and calibration using the natural fluid inclusions with known compositions.

From a sample of vein quartz containing fluid inclusions with solid phases, a piece of approx. 0.5 × 0.5 cm was chipped off. Subsequently, the fresh surface of the piece was coated with a thin layer of carbon and then studied using a Jeol-JXA 8600 electron microprobe (JEOL Ltd., Akišima, Japan) at the Department of Geology of the Palacký University in Olomouc. Backscattered electron (BSE) microphotographs of selected opened fluid inclusions were taken at an acceleration voltage of 15 kV and beam current of 10 nA, and individual phases were identified by means of EDS spectra.

Hydrogen isotopes were analyzed in selected micas and clay minerals. The impurities were manually separated from the samples under a stereoscopic binocular microscope. Then, the selected minerals were ground in an agate mortar to obtain 5–10 mg of the sample powder. Samples were analyzed following the method by [50] at Eberhard Karls Universität, Tübingen, Germany. The samples were degassed in a vacuum line at 110 °C overnight and then heated until fusion to liberate all the water. Any potentially produced H_2 was oxidized to water with a CuO trap. Water and CO_2 were separated using liquid N_2 and ethanol cold traps. Water was then reduced by Zn at approximately 400 °C, and the isotopic composition of the resulting H_2 was measured on a Finnigan MAT 252 mass spectrometer (Finnigan MAT GmbH, Bremen, Germany). The results of isotope analysis are given in δD values concerning the V-SMOW standard. The measurement error is ±2‰. The published fractionation factors were used to calculate the H isotopic composition of the fluids [51,52].

Clay minerals from the vein cavity and from the greisen surface were scraped off, dried at 50 °C for approximately 24 h and subsequently ground in an agate mortar. The powdered samples were placed on a Si wafer and dripped with isopropyl alcohol. The qualitative XRD analysis of the samples was performed on the X-ray diffractometer Bruker

D8 Advance (Bruker Co., Billerica, MA, USA) with Cu anode with variable divergent aperture screens at Θ-Θ reflective Bragg-Brentano parafocusation geometry on Research Institute for Building Materials in Brno, Czech Republic. The XRD pattern was measured in the range 2Θ = 5–100°, but subsequently, a part of the spectra was cut off due to the fact that the main peaks of clay minerals are located at low 2Θ angles. The step of the measurement was 0.020° (2Θ), and the step time was 188 s.

4. Results

4.1. Sample Types and Mineralogy

About 50 samples, including greisenized gneisses, greisenized granites, greisens, and hydrothermal veins connected with Sn-W mineralization from the Krupka ore district, were collected or borrowed to study.

Most samples were collected in the Knötel ore deposit. On the Prokop Stock, the greisenization mainly affects mantle gneisses and granites of the younger intrusive complex. Samples collected there were predominantly greisenized gneisses and quartz greisens with abundant molybdenite (Figure 2a), fluorite (Figure 2b), accessory topaz (Figure 2c), cassiterite (Figure 2d), wolframite, and apatite (Figure 2e1,e2). Greisens are, in many cases, crosscut by hydrothermal veins composed of quartz, fluorite, accessory wolframite, and sulfides. A clay mineral corresponding to dickite and less illite (confirmed by XRD analysis; Figure 3) is present in the greisens and vein cavities. Greisens from the dump material of adit Sedmi spáčů are rich in sulfides, especially chalcopyrite, which form inclusions or nests in the rock (Figure 2f). In the Preisselberg area, there are Preisselberg-type granites, which are biotite granites in places affected by greisenization (Figure 2g). Samples of greisenized granites and greisens were collected from this area. Greisens are sometimes crosscut by quartz veins up to 0.5 cm thick (Figure 2g). Many samples come from the Lukáš ore vein. Very well to perfectly limited quartz crystals (Figure 2h) reach a size up to 7 × 3 cm and have a zonal structure that is often visible to the naked eye.

Figure 4a shows a fine-grained matrix of greisen from the Preisselberg area, which is cut by a quartz vein with quartz rich in fluid inclusions. Cassiterite often shows a zonal structure (Figure 4b), showing different interference colors and pleochroism in individual zones. In samples from Knötel ore deposits this mineral encloses wolframite (Figure 4c). Micas (corresponding to protolithionite to zinnwaldite by their chemistry), enclosed in quartz, also show a zonal structure and enclose small grains of cassiterite (Figure 4d). Inclusions of wolframite often occur in cassiterite (Figure 4e). Apatite (Figure 4f) and a TiO_2 phase with a distinctly zonal structure were found in association with ore minerals (Figure 4f. The present study is based on a detailed laboratory investigation of 15 representative samples, including greisenized granites, greisens, and hydrothermal veins connected with Sn-W mineralization of the Krupka ore district (Table 1).

4.2. Petrography of Fluid Inclusions

Fluid inclusions were studied in quartz, cassiterite, topaz, fluorite, and apatite from greisens, greisenized granites, and hydrothermal veins. Fluid inclusions in quartz are very abundant. All genetic types—primary (PFI), pseudosecondary (PSFI), and secondary (SFI) fluid inclusions occur in most of the samples. In the case of topaz and apatite, fluid inclusions occur less frequently. Primary inclusions are two-phase, containing gas and aqueous components (Figure 5a). In greisens and greisenized granites, fluid inclusions (PFI1) usually have a lower degree of the filling (LVR—liquid/vapor ratio: 0.05 to 0.6) than inclusions from hydrothermal veins (0.4–0.95; PFI2). The shape of the inclusions is irregular in most cases, isometric, or less often, the inclusions have the shape of a negative crystal (Figure 5b). PFI are predominantly distributed as solitary inclusions (Figure 5c) or form small clusters. In the case of vein crystals of quartz, which have a visible growth zonation, the fluid inclusions sometimes follow the growth zones. This trend is also observed in some of the cassiterite crystals. The size of the primary inclusions varies 15–120 μm; the largest inclusions were found in quartz from greisens, and the smallest in fluorite from veins.

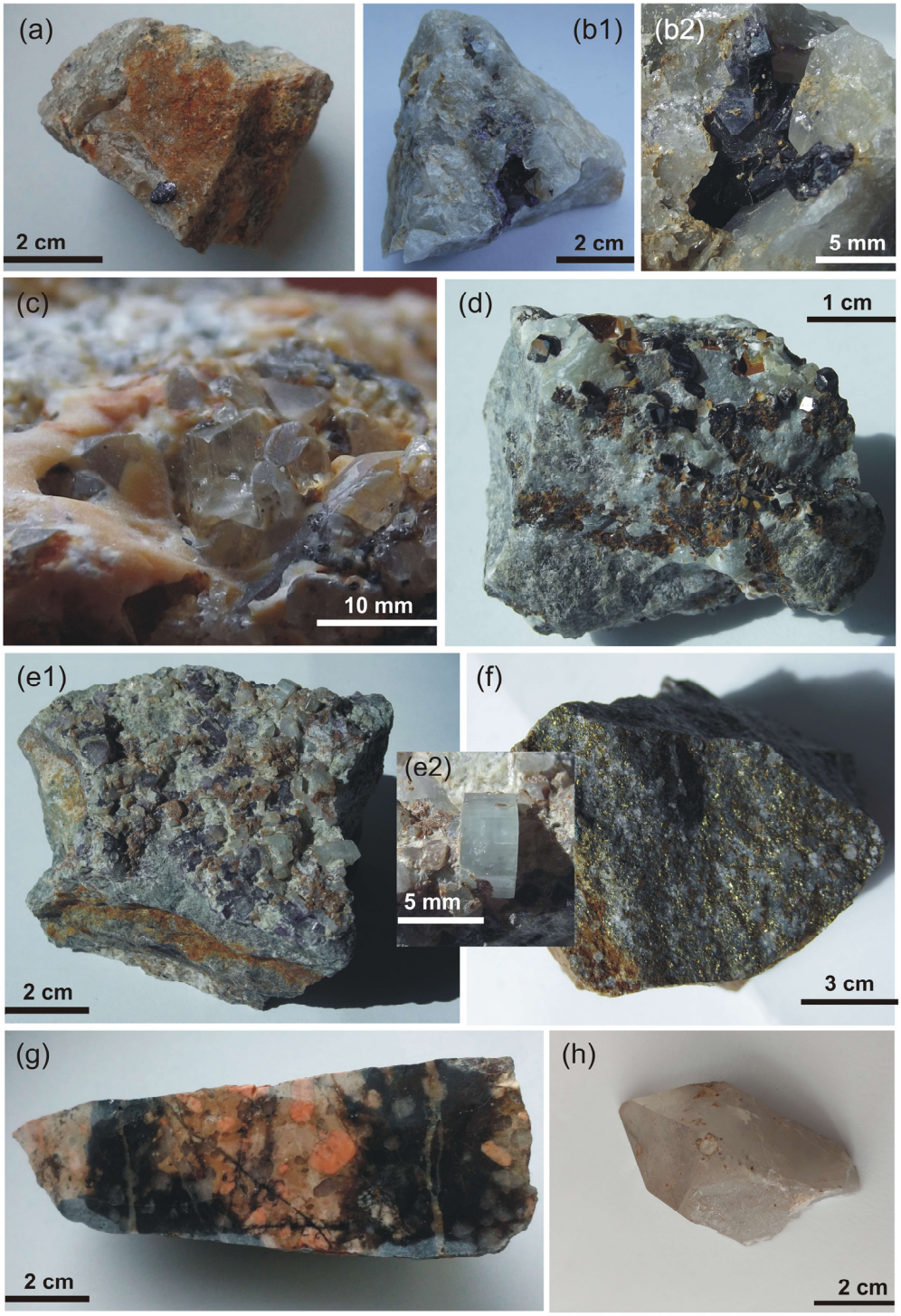


Figure 2. The texture and mineral composition of studied samples from the Krupka ore district. (**a**) Greisen sample with molybdenite from Prokop Stock, sample KR-11; (**b1**) Quartz greisen with hydrothermal vein with a cavity filled with fluorite, sample KR-12; (**b2**) Detail of cavity with fluorite crystals; (**c**) Topaz on greisen sample from Prokop Stock; sample JM-1; (**d**) Greisen sample with cassiterite from Knötel area, sample KR-10; (**e1**) Violet fluorite and light blue apatite on greisen sample from adit Martin, sample MA-3; (**e2**) Detail of apatite from (**e**); (**f**) Greisen sample with an abundant amount of sulfides, predominantly chalcopyrite from dump material from adit Sedmi spáčů, Knötel area, sample KR-3; (**g**) Sample of greisenized granite with dark greisen zones around quartz vein from Knötel area, adit Preisselberg II—sample PRK-1; (**h**) Perfectly limited crystal of quartz from Steinknochen area, Martin adit—sample KNM-3.

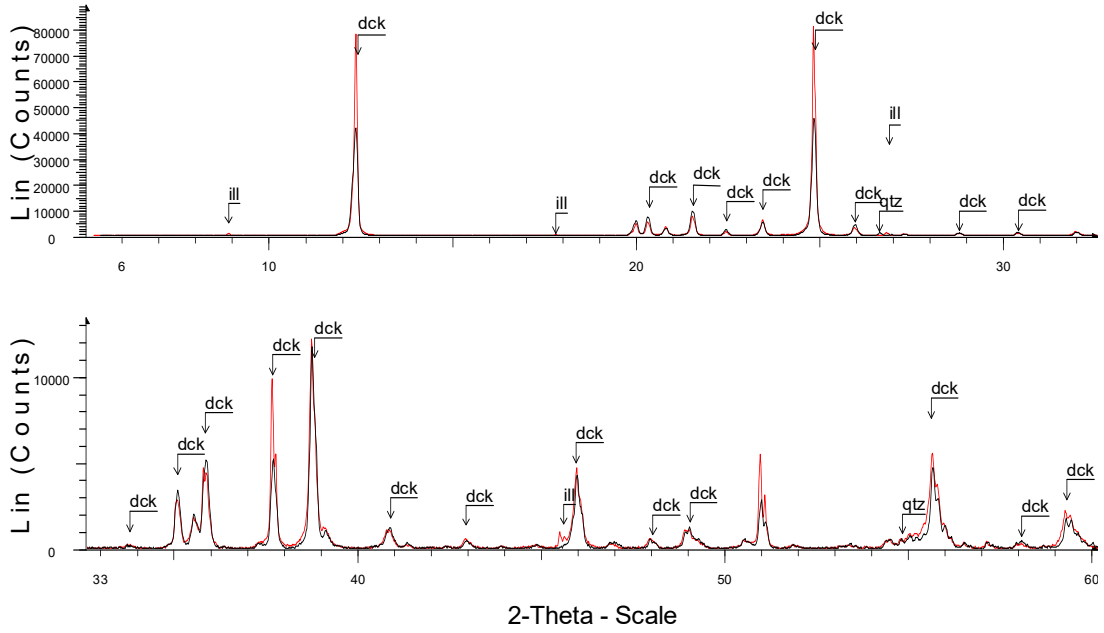


Figure 3. XRD records of clay minerals from greisen sample KR-4 (black spectrum) and hydrothermal vein sample KR-12 (red spectrum) from Knötel area; dck—dickite, ill—illite, qtz—quartz.

Table 1. List of samples from the Krupka ore district used for this study.

Sample	Locality	Type of Sample	Mineral Assemblages
KNM-1	Knötel, Prokop Stock	greisen	quartz, Li-mica, wolframite, molybdenite
KNM-2	Knötel	greisen	quartz, Li-mica, apatite, cassiterite, TiO_2 phase, wolframite
KNM-3	Steinknochen, Martin adit	hydrothermal vein	quartz, oxi-hydroxides of Fe
KNM-4	Knötel	greisen	quartz, Li-mica, wolframite
KR-17	Knötel	greisenized granite	quartz, micas, K-feldspar, plagioclase, cassiterite,
KR-3	Knötel, adit Sedmi spáčů	greisen	quartz, Li-mica, cassiterite, wolframite, chalcopyrite, pyrite, galena, arsenopyrite
KR-4	Knötel	greisen	quartz, Li-mica, wolframite, dickite, illite, fluorite
KR-5	Knötel	greisen	quartz, protolithionite/zinnwaldite, cassiterite
KR-7	Knötel	greisen	quartz, phengite/Li-phengite, molybdenite, fluorite, woframite
KR-8	Knötel, Prokop Stock	greisen	quartz, molybdenite, wolframite, fluorite, dickite
KR-10	Knötel, Prokop Stock	greisen	quartz, Li-mica, cassiterite, wolframite
KR-11	Knötel, Prokop Stock	greisen	quartz, mica, molybdenite, Bi-minerals
KR-12	Knötel, Prokop Stock	greisen	quartz, wolframite, fluorite, clay minerals
KR-12	Knötel, Prokop Stock	hydrothermal vein	quartz, fluorite, clay mineral
PRK-1	Preisselberg	greisenized granite	quartz, plagioclase, K-feldspar, Li-mica, cassiterite, zircon
PRK-1	Preisselberg	greisen	quartz, Li-mica, zinnwaldite, muscovite, cassiterite, topaz
PRK-1	Preisselberg	hydrothermal vein	quartz

Pseudosecondary inclusions (PSFI) occur mainly in quartz from greisenized granites, greisen, and veins. They are found less frequently in cassiterite and fluorite (Figure 5d) and were not detected in topaz and apatite. PSFIs are two-phase, gas-liquid with LVR 0.3 to 0.95 and reach a maximum size of 45 µm. Two types of pseudosecondary inclusions were distinguished according to their degree of filling (PSFI1-LVR: 0.3–0.7; PSFI2-LVR: 0.7–0.95). PSFIs often have an irregular or oval shape. Inclusions with a negative crystal shape and drop-like-shaped inclusions occur less often. The distribution of inclusions is as short trails not passing through the whole grains or forming small clusters. Inclusions often have varying degrees of filling, especially in quartz from greisens (Figure 5e).

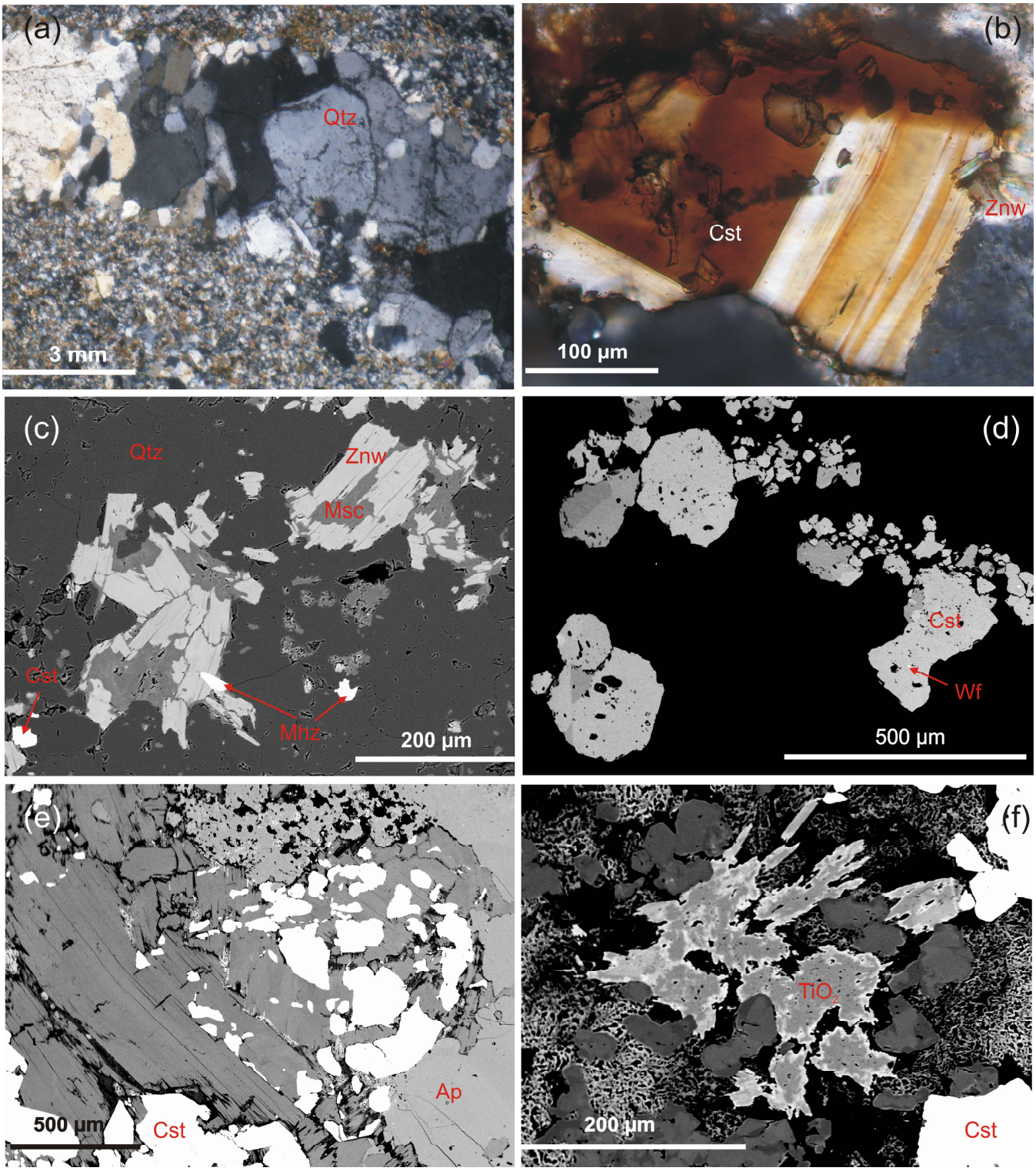


Figure 4. Mineral assemblages and texture of the samples. (**a**) Greisen from Preisselberg (sample PRK-1) cut by quartz vein (Qtz), polarized light, XPL; (**b**) Grain of cassiterite (Cst) with zonal structure and zinnwaldite (Znw) fan-like crystals in greisenized granite from Preisselberg (PRK-1), polarized light, XPL; (**c**) Zonal tabular crystals of micas corresponding to muscovite (Msc) and zinnwaldite (Znw) enclosed in quartz (Qtz) from greisen (PRK-1), BSE image; (**d**) Wolframite grains enclosed in cassiterite, BSE image; (**e**) Cassiterite (Cst) in mica interlayers and in association with apatite (Ap) from greisen from Knötel–Prokop Stock (KNM-2), BSE image; (**f**) Zonal TiO_2 phase in association with quartz and cassiterite (Cst) in greisen from Knötel–Prokop Stock (KNM-2), BSE image.

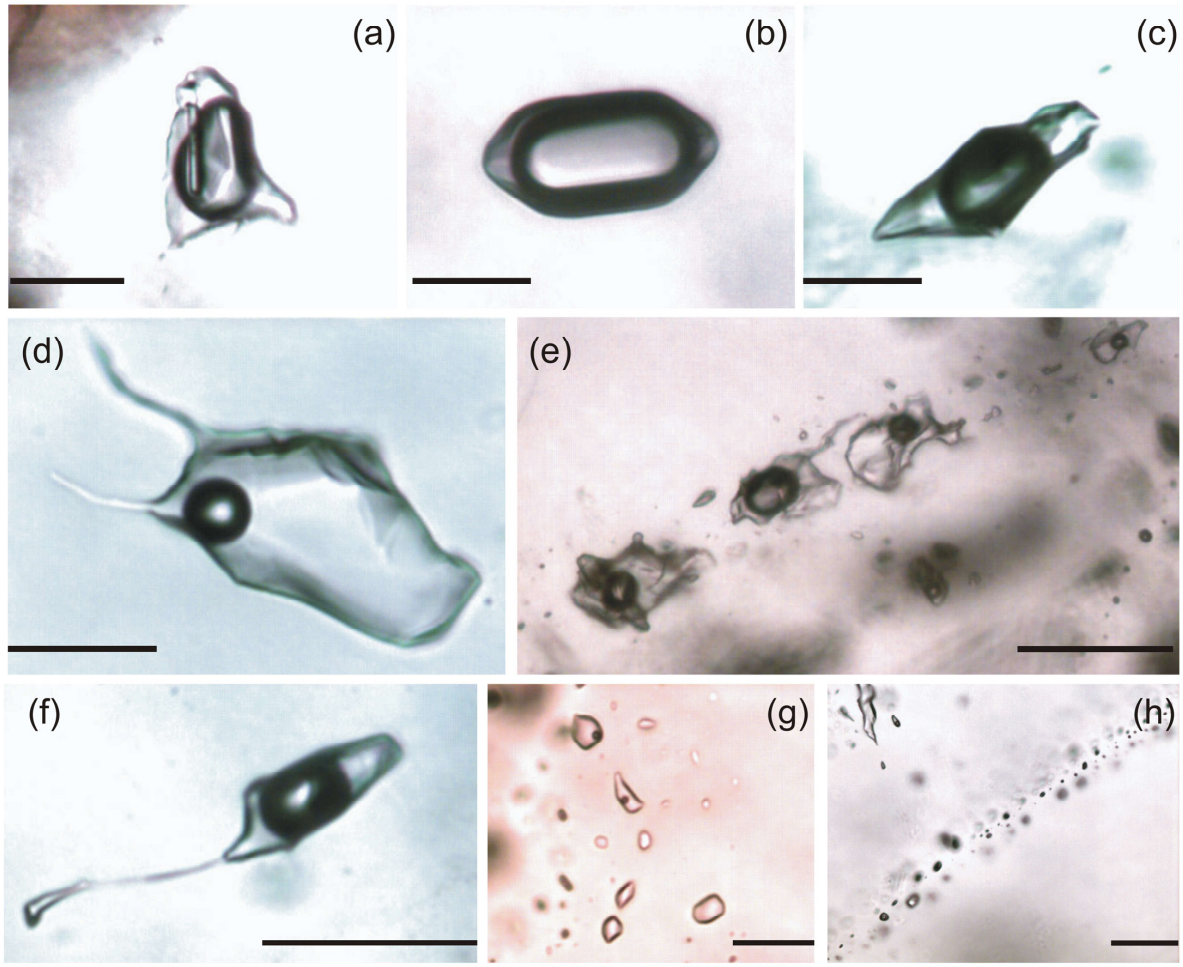


Figure 5. Appearance of fluid inclusions in minerals from the Krupka ore district in polarized light (PPL) at room temperature: (**a**) Primary inclusion from topaz from greisen sample KNM-2; (**b**) Vapor-rich negative crystal-shaped primary fluid inclusions from quartz from greisen sample KR-11 from Knötel; (**c**) Solitary primary fluid inclusion from quartz from vein sample KNM-3; (**d**) Pseudosecondary inclusion from fluorite from vein sample KR-12; (**e**) Short trail of pseudosecondary inclusions from quartz from greisen with variable LVR, sample KR-12; (**f**) Secondary inclusion from quartz from greisenized granite affected by necking-down, sample PRK-1; (**g**) Group of secondary liquid and liquid-vapor fluid inclusions from greisen, sample KR-12; (**h**) Trail of secondary inclusions from vein quartz; sample PRK-1. Scale bar is 20 μm for all microphotographs.

For secondary inclusions, three types were distinguished, differing in the degree of filling and the presence of solid phases enclosed in inclusions. Secondary inclusions of the first type (SFI1) occur in quartz and less often in cassiterite from greisen and greisenized granites. They have a lower LVR (0.4–0.95) than inclusions of the second type (SFI2; LVR 0.7–1.0), which occur predominantly in vein minerals. SFI1 inclusions are situated on cracks and form trails that mostly cross the whole grains; sometimes, they continue through the neighboring grain. Secondary inclusions in quartz and cassiterite are often affected by the necking-down (Figure 5f). Stretched inclusions with varying degrees of filling often occur side by side, with some inclusions containing liquid phase. SFI2 inclusions are two-phase but quite often are also single-phase, containing only the liquid phase. SFI2 inclusions are usually smaller than SFI1, and the shape of the inclusions is oval, spherical, or irregular. Inclusions form small groups on cracks (Figure 5g,h) and occur predominantly in quartz, less often in cassiterite and fluorite. The youngest generation of SFI2 are fluid inclusions that intersect whole grains and sometimes also several grains, have a high degree of filling, and often are all-liquid. Opaque SFI1 or PSFI1 were found in some samples of

cassiterite. The third type of secondary inclusions (SFI3) contains, in addition to the gaseous and aqueous phase, one or more solid phases (Figure 6a–j) and is only found in quartz (Figure 6a–i) and cassiterite (Figure 6j). The amount of vapor phase in this type of inclusion does not exceed 50 vol. %. The shape of the inclusions is irregular, or the inclusions have the shape of a negative crystal (Figure 6a,i). Inclusions reach up to 70 μm in size. SFI3 inclusions occur on trails crossing the grains. Some multiphase inclusions occur as solitary inclusions, and some may also perhaps be classified as pseudosecondary inclusions. SFI3 forming short trails composed of only a few inclusions often exhibit decreasing sizes of inclusions toward the grain core, indicating the healing of small cracks in the minerals. In a few cases of FI on cracks, these inclusions have different degrees of filling, with inclusions toward the grain edge having a higher content of the gaseous phase than inclusions toward the grain core. As far as the age of SFI3, it seems most likely that the solitary or small group inclusions represent the older generation of SFI3, followed by inclusions healing small cracks or forming trails intersecting whole grains. Older solitary multiphase inclusions have a large size and often contain more solid phases than inclusions on trails.

Identification of some solids in SFI3 inclusions was performed by microthermometric measurements; other phases were identified by Raman spectroscopy and EDS analysis. Quartz, carbonates (calcite, siderite), and an unspecified sulfate were identified by Raman spectroscopy. The Raman spectrum of one of the analyzed carbonates is shown in Figure 7. An intense peak at 1085 cm^{-1} and a less intense one at 736 cm^{-1} correspond with a high probability of siderite, according to [49]. An unspecified sulfate has the shape of needles with dimensions of approximately 9 × 1 μm. It was found in only one quartz-hosted secondary inclusion from the vein sample KR-12. The Raman spectrum of this phase is characterized by peaks at 449, 1001, and 1064 cm^{-1}. It is quite difficult to identify chlorides using Raman spectroscopy, as they often have only a weak signal and in combination with strong fluorescence, identification is often impossible. A vein quartz sample from Prokop Stock was studied using an electron microprobe focusing on fluid inclusions containing solid phases. The EPMA revealed the presence of quartz (Figure 6k), topaz (Figure 6l), galena, and an unspecified Na-Al silicate. Multiphase inclusions enclosing quartz reach a size of up to 30 μm and form a short trail. Quartz is present in all inclusions in the trail (Figure 6k). Topaz forms a columnar, perfectly confined crystal (Figure 6l). A Na-Al silicate is in the form of needles up to 25 μm long. More than 10 needles of this phase occur in the inclusion.

4.3. Microthermometry of Fluid Inclusions

The results of microthermometric measurements are shown in Figure 8a–d and Table 2. The homogenization to liquid or vapor and, in some cases, also critical homogenization was observed in primary fluid inclusions. The latter type of homogenization was frequently observed in quartz from greisens and also, in a few cases, in apatite, cassiterite, and topaz. The highest homogenization temperatures were measured in PFI1 hosted by cassiterite, quartz, and topaz (Figure 8a), with higher temperatures recorded for homogenization to vapor (356–498 °C) than in case of critical homogenization (389–421 °C) and homogenization to liquid (336–441 °C) (Table 2). Pseudosecondary and secondary inclusions homogenize to liquid in many cases; only a few inclusions, which have a low degree of filling, homogenize to vapor. The lowest homogenization temperatures were measured for fluorite (Table 2, Figure 8a). The dark opaque pseudosecondary/secondary inclusions in cassiterite did not react to heating or cooling, as no phase transitions were visible. Halite in PSFI/SFI3 dissolves in a wide range of temperatures from 120 to 335 °C, and the total homogenization temperature of SFI3 inclusions with halite is in the range 141 to 369 °C (Figure 9, Table 3). In the Th vs. Tds_H plot, the data points are located below and above the diagonal reference 1:1 line (Figure 9). The SFI3 from greisens shows a wider range of Tds_H values than inclusions from greisenized granites and veins and, consequently, also has a wider range of salinities (Figure 9). Halite-bearing SFI3 from hydrothermal veins homogenizes on average at lower temperatures than SFI3 from greisens and greisenized granites. In a few cases of multiphase SFI3 inclusions, decrepitation occurred before the inclusion was homogenized. The phase

transitions during heating of a multiphase inclusion from vein quartz of sample KNM-3 are illustrated in Figure 10. At room temperature, the inclusion contains a gas bubble, aqueous liquid, and four solid phases, one of which is halite, which disappears at a temperature of 268 °C and then the inclusion homogenizes into a liquid at a temperature of 370 °C. Other solid phases dissolve at very low temperatures, up to 60 °C (Figure 10).

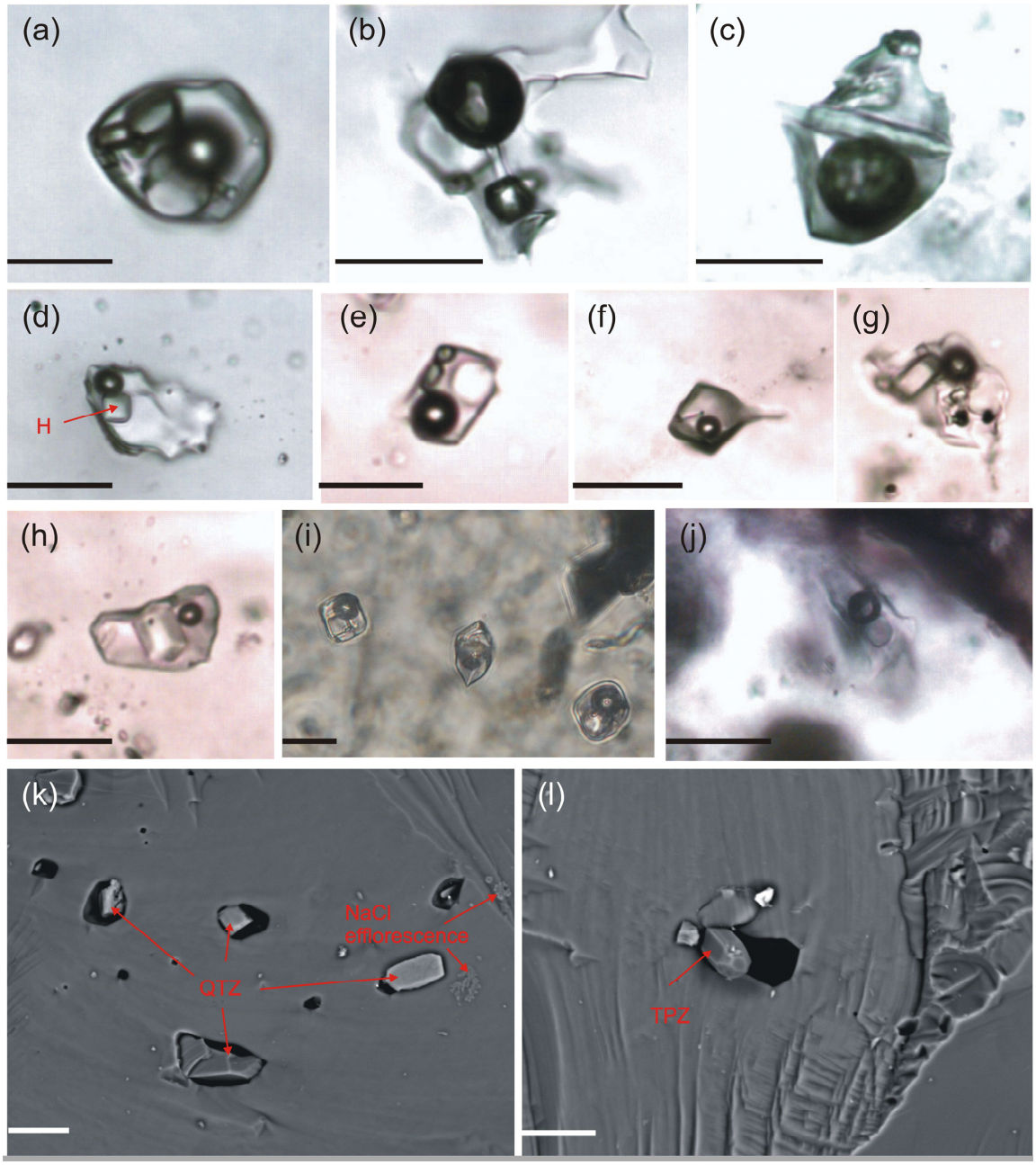


Figure 6. Appearance of multiphase pseudosecondary/secondary fluid inclusions with solid phases in quartz from greisen sample KR-12 (**a**–**d**) and KR-11 (**e**–**h**) from Prokop Stock, trail of multiphase SFI3 inclusions from quartz from vein sample KNM-3 (younger generation of SFI3); (**i**) from Steinknochen (Martin adit) and cassiterite from greisenized granite (sample PRK-1) from Preisselberg (**j**) under the microscope in polarized light at room temperature (PPL), H—halite; fluid inclusions in quartz from greisen sample KR-12 in BSE: (**k**) Group of opened fluid inclusions in quartz from greisen sample KR-12 from Prokop Stock with grains of quartz (QTZ); (**l**) Fluid inclusion in quartz from greisen sample KR-12 from Prokop Stock encloses crystal of topaz (TPZ); scale bar is 20 μm for all microphotographs.

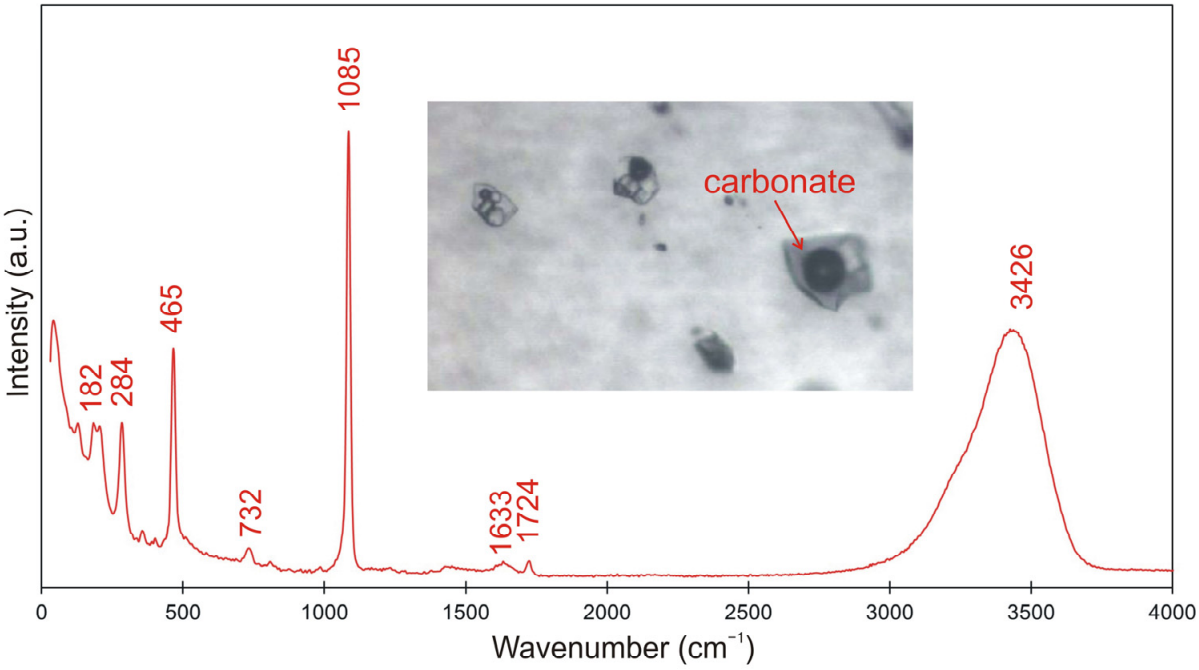


Figure 7. Raman spectrum of a solid carbonate enclosed in a multiphase SFI3 from vein quartz from Krupka (sample KMN-3). The size of the studied inclusion is 27 μm.

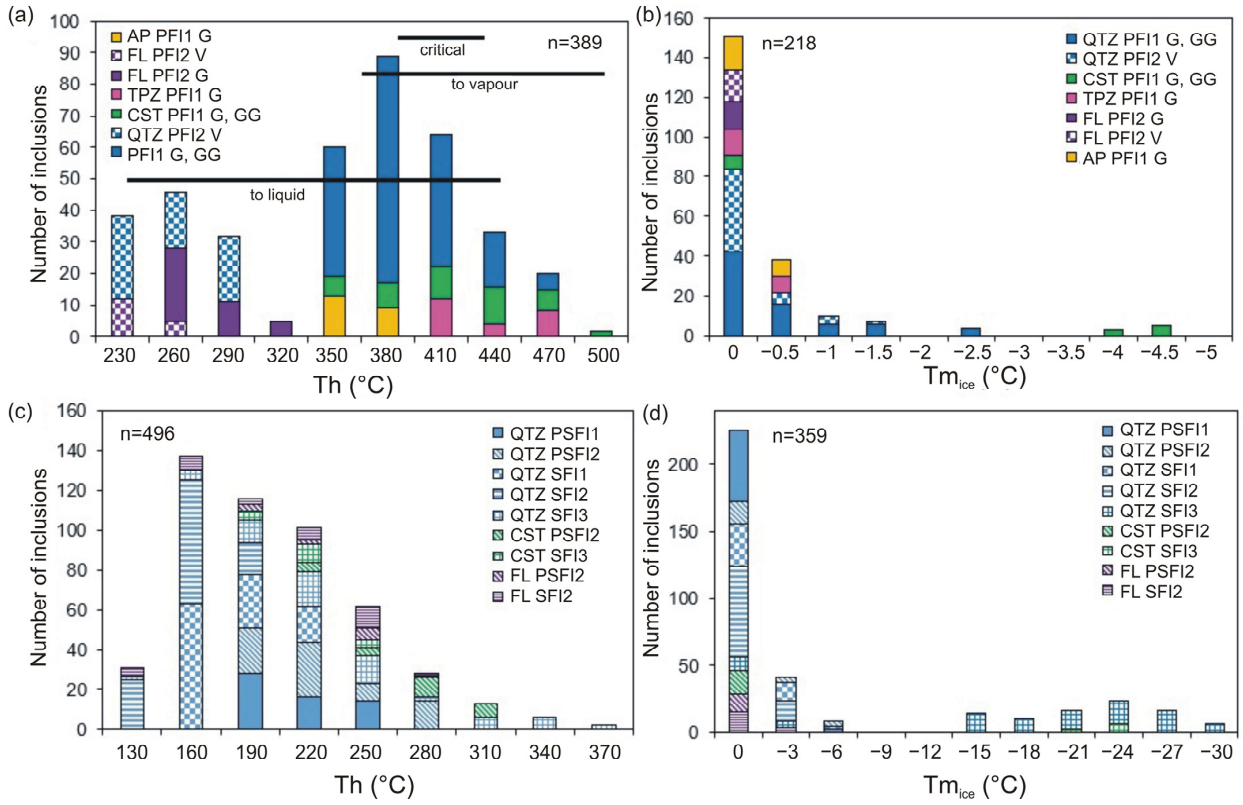


Figure 8. Histograms of homogenization temperatures and ice melting temperatures of fluid inclusions from Krupka, G—greisens, GG—greisenized granites, V—veins: (**a**) Homogenization temperatures of primary inclusions, bars indicate the ranges for individual modes of homogenization; (**b**) Ice melting temperatures of primary inclusions; (**c**) Homogenization temperatures of pseudosecondary and secondary fluid inclusions; (**d**) Ice melting temperatures of pseudosecondary and secondary inclusions.

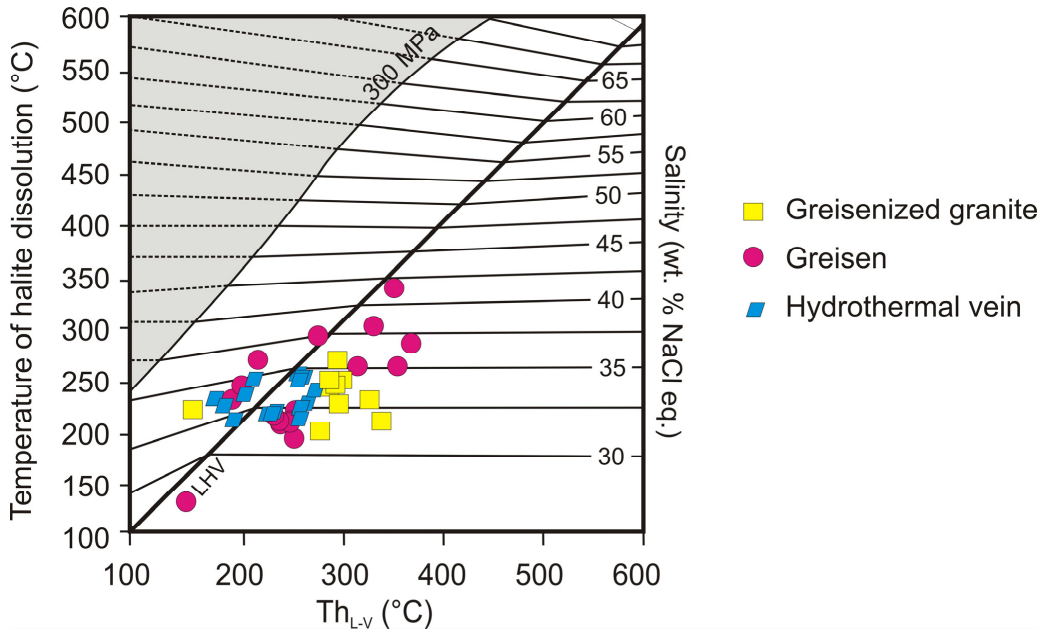


Figure 9. Plot Th vs. Tds_H vs. salinity (model) after [53] with data points of SFI3 from the Krupka ore district.

Table 2. Results of microthermometric measurements of fluid inclusions from the Krupka ore district.

Sample	Mineral	No. of FI	Genesis	Phase Composition	LVR	Th_L (°C)	Th_V (°C)	Th_C (°C)	Tm_{ice} (°C)	Te (°C)
Greisenized granite										
PRK-1	qtz	17	PFI1	L+V	0.05–0.6	351–441	392–456	-	−2.5 to 0	−22.8 to −23.0
PRK-1	qtz	15	PSFI1	L+V	0.4–0.7	236–252	247–265	-	−1.5 to 0	-
PRK-1	qtz	14	PSFI2	L+V	0.7–0.95	178–295	-	-	−5.2 to 0	-
PRK-1	qtz	13	SFI1	L+V	0.4–0.95	156–234	-	-	−3.5 to 0	-
PRK-1	qtz	14	SFI2	L+V	0.8–0.95	115–205	-	-	−0.6 to 0	-
PRK-1	cst	14	PFI1	L+V	0.1–0.5	362–423	396–498	-	−0.2 to 0	-
PRK-1	cst	9	PSFI2	L+V	0.7–0.95	208–311	-	-	−1.5 to 0	-
PRK-1	cst	-	SFI1/PSFI1	V (?)	-	-	-	-		-
KR-17	qtz	13	PFI1	L+V	0.05–0.5	342–416	382–421	-	−2.5 to 0	−22.8
KR-17	qtz	11	PSFI2	L+V	0.7–0.95	182–235	-	-	−0.8 to 0	−23.0 to −23.1
KR-17	qtz	8	SFI1	L+V	0.4–0.95	165–228	-	-	−3.3 to 0	-
KR-17	qtz	12	SFI2	L+V	0.7–0.95	117–192	-	-	−0.3 to 0	-
KR-17	cst	9	PFI1	L+V	0.2–0.5	378–435	363–465	-	−4.6 to −0.1	
Greisen										
PRK-1	qtz	24	PFI1	L+V	0.1–0.6	377–401	392–425	389–412	−2.3 to −0.1	-
PRK-1	qtz	13	PSFI1	L+V	0.3–0.6	205–249	-	-	−1.3 to 0	-
PRK-1	qtz	8	PSFI2	L+V	0.7–0.95	231–282	-	-	−3.6 to 0	-
PRK-1	qtz	16	SFI1	L+V	0.5–0.9	149–227	-	-	−4.0 to 0	-
PRK-1	qtz	15	SFI2	L, L+V	0.7–1.0	121–199	-	-	−2.6 to −0.1	−23
PRK-1	cst	16	PFI1	L+V	0.1–0.5	362–425	383–406	-	−0.2 to 0	-
PRK-1	cst	8	SFI2	L+V	0.7–0.95	145–201	-	-		
PRK-1	tpz	16	PFI1	L+V	0.05–0.6	393–423	408–456	401–416	−0.7 to 0	-
KR-3	qtz	16	PFI1	L+V	0.2–0.5	367–402	398–431	406, 413	−2.1 to 0	
KR-4	qtz	14	PFI1	L+V	0.1–0.5	345–387	376–469		−0.8 to −0.1	
KR-4	fl	9	PFI2	L+V	0.7–0.9	224–289	-	-	−0.2 to 0	-
KR-5	qtz	10	PFI1	L+V	0.2–0.5	354–421	382–439		−2.0 to 0	
KR-7	qtz	10	PFI1	L+V	0.2–0.6	372–418	390–447		−1.5 to 0	
KR-8	qtz	12	PFI1	L+V	0.1–0.5	345–421	364–473		−2.5 to −0.2	
KR-8	fl	11	PFI2	L+V	0.7–0.95	254–296	-	-	−0.1 to 0	-
KR-11	qtz	31	PFI1	L+V	0.1–0.5	357–406	370–428	397–409	−0.5 to 0	
KR-12	qtz	27	PFI1	L+V	0.1–0.5	348–411	381–489	397–421	−2.1 to −0.2	−22.8
KNM-1	qtz	18	PFI1	L+V	0.1–0.5	383–396	356–402		−2.3 to 0	
KNM-4	qtz	15	PFI1	L+V	0.2–0.5	361–380	377–421		−1.7 to −0.1	
KR-11	qtz	8	PSFI1	L+V	0.5–0.7	208–232	-	-	−1.0 to 0	-

Table 2. *Cont.*

Sample	Mineral	No. of FI	Genesis	Phase Composition	LVR	Th_L (°C)	Th_V (°C)	Th_C (°C)	Tm_{ice} (°C)	Te (°C)
KR-12	qtz	12	PSFI1	L+V	0.5–0.7	203–212	-	-	−0.5 to 0	-
KNM-1	qtz	6	PSFI1	L+V	0.5–0.7	216–262	-	-	−0.3 to 0	-
KR-12	qtz	11	PSFI2	L+V	0.8–0.95	201–232	-	-	−3.1 to 0	-
KR-11	qtz	21	SFI1	L+V	0.6–0.8	190–213	-	-	−2.5 to 0	-
KR-12	qtz	28	SFI1	L+V	0.5–0.8	175–209	-	-	−3.2 to 0	-
KNM-1	qtz	7	SFI1	L+V	0.6–0.7	169–193	-	-	−4.0 to −0.2	-
KR-5	qtz	13	SFI2	L+V	0.8–0.95	116–186	-	-	−4.2 to 0	−37.7
KR-11	qtz	21	SFI2	L, L+V	0.8–1.0	145–174	-	-	−2.5 to −0.3	−38.4
KR-12	qtz	28	SFI2	L, L+V	0.8–1.0	121–206	-	-	−5.8 to 0	−37.3, −37.5
KNM-1	qtz	9	SFI2	L, L+V	0.8–1.0	139–152	-	-	−0.4 to 0	
KNM-4	qtz	11	SFI2	L, L+V	0.8–1.0	119–128	-	-	−0.2 to 0	
KR-5	cst	10	PFI1	L+V	0.1–0.5	352–440	376–462	-	−0.2 to 0	-
KR-10	cst	14	PFI1	L+V	0.2–0.6	336–412	399–403	-	−0.1 to 0	-
KR-5	cst	7	PSFI2	L+V	0.8–0.95	246–289	316–322	-	−2.8 to 0	-
KR-10	cst	-	SFI1	L+V, V (?)	0–0.05 (?)	-	-	-		-
KNM-2	tpz	8	PFI1	L+V	0.2–0.5	398–431	405–416	412–423	−0.4 to 0	-
KNM-2	ap	21	PFI1	L+V	0.1–0.5	342–390	-	-	−0.5 to 0	−22.8 to −22.9
KR-11	fl	12	PFI2	L+V	0.6–0.9	216–301	-	-	−0.2 to 0	-
KR-11	fl	6	PSFI2	L+V	0.8–0.95	176–241	-	-	−1.3 to 0	-
KR-11	fl	13	SFI2	L+V	0.7–0.95	121–247	-	-	−2.1 to 0	-
				Hydrothermal vein						
KNM-3	qtz	23	PFI2	L+V	0.5–0.9	218–291	-	-	−1.1 to 0	
KNM-3	qtz	4	PSFI1	L+V	0.5–0.7	213–266	-	-	−1.2 to 0	-
KNM-3	qtz	12	PSFI2	L+V	0.8–0.95	177–242	-	-	−6.5 to 0	-
KNM-3	qtz	13	SFI1	L+V	0.4–0.9	165–230	-	-	−3.5 to 0	-
KNM-3	qtz	21	SFI2	L+V	0.7–0.95	<50–201	-	-	−2.6 to 0	-
KR-12	qtz	42	PFI2	L+V	0.4–0.7	256–302	-	-	−0.4 to 0	−22.9
KR-12	qtz	17	PSFI2	L+V	0.8–0.95	199–245	-	-	−1.5 to 0	-
KR-12	qtz	21	SFI1	L+V	0.7–0.9	160–202	-	-	−3.5 to 0	-
KR-12	qtz	32	SFI2	L, L+V	0.8–0.95	137–182	-	-	−4.5 to 0	−36.3 to −37.9
KR-12	fl	14	PFI2	L+V	0.7–0.95	247–276	-	-	−0.2 to 0	-
KR-12	fl	16	SFI2	L+V	0.95	115–204	-	-	−3.8 to 0	-
KR-8	fl	6	PFI2/PSFI1	L+V	0.7–0.95	191–213			−0.3 to 0	
PRK-1	qtz	26	PFI2	L+V	0.5–0.8	259–279	-	-	−1.2 to 0	-
PRK-1	qtz	8	SFI1	L+V	0.7–0.9	148–223	-	-	−2.8 to 0	-
PRK-1	qtz	14	SFI2	L, L+V	0.9–1.0	<50–162	-	-	−1.3 to 0	-

Table 3. Results of microthermometric measurements of multiphase inclusions from the Krupka ore district.

Sample	Mineral	Genesis	No. of FI	Phase Composition	LVR	Th_L (°C)	Tm_{ice} (°C)	Tds_h (°C)
				Greisenized granite				
PRK-1	qtz	PSFI/SFI3	6	L+V+S	0.6–0.95	151–303	−31.0 to −14.1	162–202
PRK-1	cst	PSFI/SFI3	8	L+V+S	0.5–0.9	293–335	−25.5 to −19.5	178–224
				Greisen				
PRK-1	qtz	PSFI/SFI3	12	$L+V+S_{1–3}$	0.7–0.95	263–369	−26.1 to −15.2	189–314
KR-3	cst	PSFI/SFI3	6	$L+V+S_{1–3}$	0.5–0.95	141–327	−23.2 to −21.7	145–335
KR-12	qtz	PSFI/SFI3	15	$L+V+S_{1–6}$	0.5–0.95	196–242	−27.6 to −16.0	182–281
KNM-1	qtz	PSFI/SFI3	9	$L+V+S_{1–6}$	0.6–0.95	189–221	−28.1 to −18.3	178–204
KR-11	qtz	PSFI/SFI3	17	$L+V+S_{1–5}$	0.5–0.95	212–248	−25.8 to −20.4	210–270
KR-11	qtz	SFI3	4	L+V+S	0.8–0.95	182–311	−1.3 to −0.2	-
KR-10	cst	PSFI/SFI3	5	$L+V+S_{1–2}$	0.7–0.95	192–245	−24.5 to −19.7	214–275
				Hydrothermal vein				
KNM-3	qtz	PSFI/SFI3	16	$L+V+S_{1–5}$	0.6–0.95	164–213	−26.5 to −17.2	201–251
KR-12	qtz	SFI3	8	$L+V+S_{1–2}$	0.7–0.95	126–362	−3.0 to 0	-
KR-12	qtz	PSFI/SFI3	14	$L+V+S_{1–6}$	0.6–0.95	182–265	−30.8 to −14.3	192–231

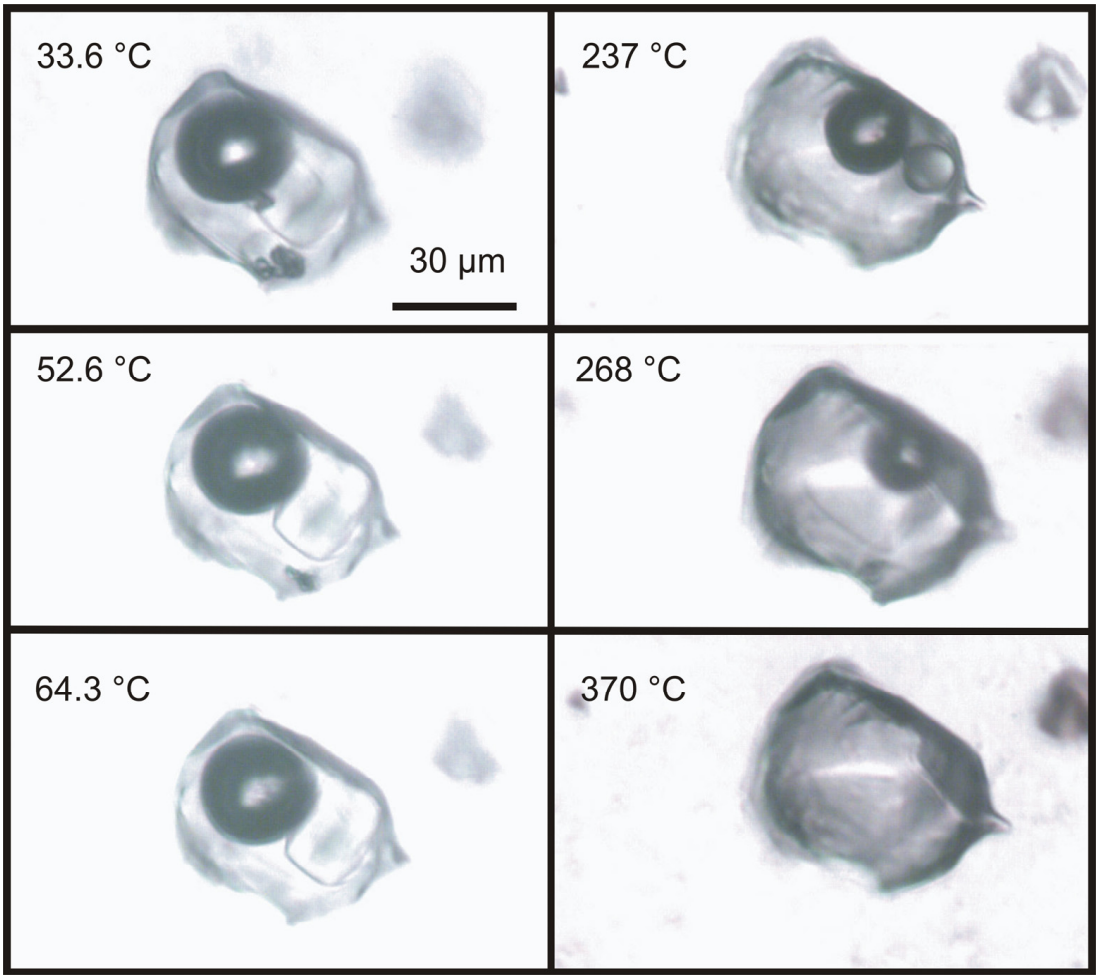


Figure 10. Example of phase transitions during heating of a PSFI/SFI3 fluid inclusion from vein quartz from sample KNM-3 (Lukáš vein, Martin adit).

In the cooling mode, the freezing temperatures of FI range from −18 to −62 °C. In several cases of PFI in quartz samples from greisens with low LVR and in some PSFI/SFI3 with solid phases, the inclusions did not freeze even when cooled to −120 °C. During heating of the frozen inclusions, the eutectic temperature was occasionally measured, which ranged from −22.8 to −23.2 °C in most cases, and for a few secondary inclusions in quartz from greisens and veins, it varies from −36.3 to −38.4 °C (Table 2). The last ice crystal melts in most primary inclusions at temperatures −1.5 to 0 °C, rarely down to −2.6 °C (for quartz) and −4.6 °C (for cassiterite), which corresponds to salinity 0 to 7.3 wt. % NaCl eq. The last ice crystal in pseudosecondary and secondary inclusions also melts mostly in the range of −3 to 0 °C, less often down to −6 °C for quartz (Figure 8d). Exceptions are PSFI/SFI3 from quartz and cassiterite with solid phases that showed Tm_{ice} values at much lower temperatures (down to −31 °C; Table 3, Figure 8d). In some PSFI multiphase inclusions, where the ice melted at low temperatures, the melting of hydrohalite was observed at temperatures around 2–5 °C in quartz from sample KNM-3. SFI3, which does not contain crystals of halite but usually contains one other phase (topaz, quartz, sulfides or other opaque minerals) present in several samples of quartz from greisens and veins. These inclusions show a melting temperature of the last ice crystal from −3 °C to 0 °C (Table 3). Solitary multiphase PSFI mostly shows lower temperatures of ice melting than inclusions on trails.

The system H_2O-gases-salts was recognized only in primary and pseudosecondary inclusions of a few samples of quartz, cassiterite, and topaz from greisens. Inclusions with a low degree of filling, in most cases, homogenize to vapor; inclusions with a dominant liquid

phase usually homogenize to liquid. In several cases, critical homogenization has also occurred. Fluid inclusions containing gases are two-phase at room temperature, and the condensation of the liquid carbonic phase was not observed during cooling runs. In some inclusions, however, the presence of gases was identified by the crystallization of clathrate. Clathrate dissociates at temperatures between 4.2 and 10.1 °C, with higher temperatures measured for cassiterite from sample PRK-1 (Table 4). The total homogenization temperatures of clathrate-bearing inclusions do not differ significantly from the homogenization temperatures of inclusions without detectable gases.

Table 4. Results of microthermometry of clathrate-bearing inclusions from Krupka ore district.

Sample	Mineral	Genesis	No. of FI	Phase Composition	LVR	Th_L (°C)	Th_V (°C)	Thc (°C)	Tm_{ice} (°C)	Tm_{cla} (°C)
PRK-1	cst	PFI1/PSFI1	4	L+V	0.1–0.4	-	399–456		−0.2 to 0	5.6–10.1
KR-5	cst	PFI1	2	L+V	0.1–0.3	-	396, 402		−0.1 to 0	4.8, 6.1
KR-12	qtz	PFI1	2	L+V	0.1–0.3	-	392	408	−2.1 to 0	4.2, 4.7
KNM-1	qtz	PFI1	2	L+V	0.2–0.4	-	422,438		−0.8 to 0	5.8, 7.3
KNM-2	qtz	PFI1	5	L+V	0.1–0.5	389, 401	406–419		−1.4 to −0.1	4.2–7.3
KNM-2	tpz	PFI1	7	L+V	0.2–0.5	399–413	403–408	401	−0.6 to 0	4.4–8.4

4.4. Composition of Vapor Phase

Raman spectroscopy of gaseous FI in quartz from greisen (KR-12) and vein (KNM-3) samples was performed. Only CO_2 was identified by Raman analysis in a primary inclusion. In another PFI from greisen, trace amounts of N_2 (1.7 mol. %) and CH_4 (2.1 mol. %) were recorded in addition to CO_2 (96.2 mol. %). An example of the Raman spectrum of gaseous phases in fluid inclusions hosted by quartz from greisen is shown in Figure 11. In the quartz sample from the Lukáš vein, gaseous phases were analyzed in three pseudosecondary/secondary fluid inclusions. A higher CH_4 content (28.8 and 100 mol. %) was recorded in two inclusions; the nitrogen content is either none or negligible (0.1 mol. %). The rest of the non-aqueous phase is CO_2. The results are presented in Table 5.

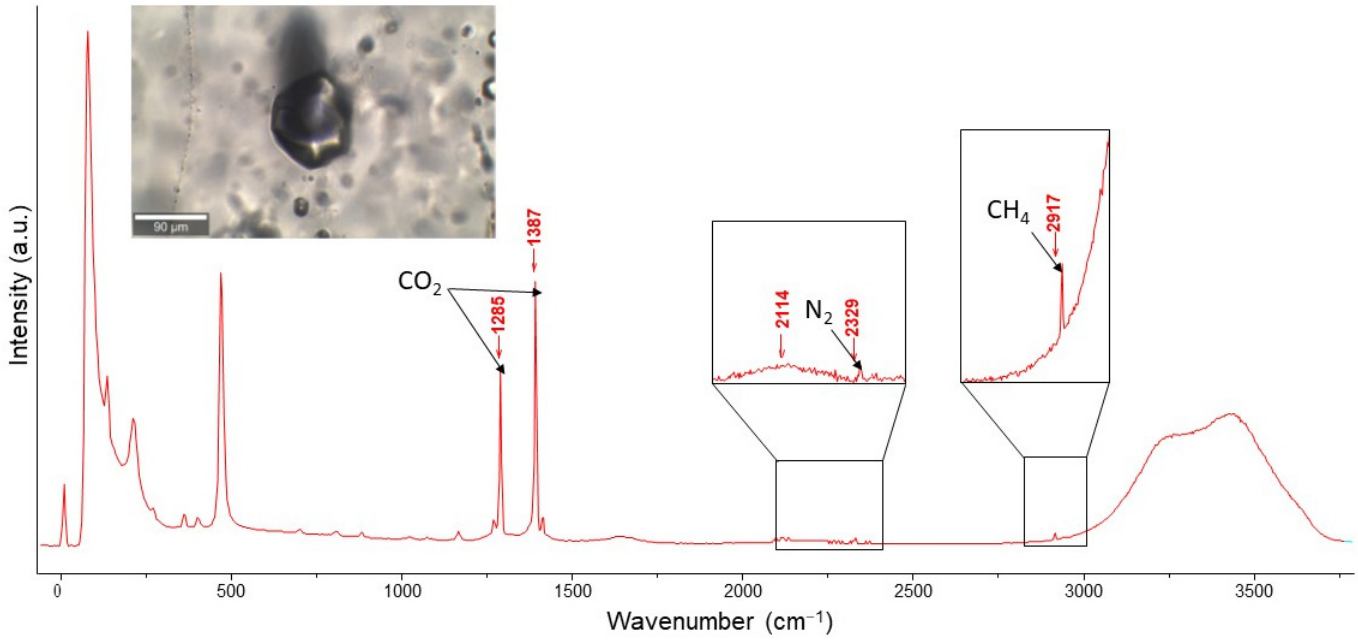


Figure 11. Raman spectrum of gaseous phase enclosed in a primary fluid inclusion from quartz in greisen from Krupka (KR-12).

Table 5. Composition of non-aqueous phase in fluid inclusions from the Krupka ore district.

			CH_4	CO_2	N_2
Sample	**Mineral**	**Genesis**		**mol. %**	
KNM-3	qtz	PFI2/PSFI1	28.8	71.1	0.1
KNM-3	qtz	PFI2/PSFI1	1.3	98.7	0
KNM-3	qtz	PFI2/PSFI1	100	0	0
KR-12	qtz	PFI1	0	100	0
KR-12	qtz	PFI1	2.1	96.2	1.7

4.5. Crush-Leach Analyses of Fluid Inclusions

Fluid inclusion leachates of three quartz samples were analyzed: one from greisen with fluorite, the second from greisen with molybdenite, and the last from a hydrothermal vein. The dominant cation is Na^+ in leachate from quartz from greisen with fluorite and vein quartz, while Ca predominates in leachate from greisen with molybdenite. The Na/K ratio is lowest for greisen with molybdenite and highest for quartz from a vein. The highest Mg contents are present in the quartz sample from greisen with molybdenite. Cl^- is the dominating anion in all leachates. The content of nitrates in greisen with molybdenite is also relatively high and more than 4.5 times higher than in leachate from vein quartz (Table 6). The contents of Li, Br, I, and F are relatively low (Table 6). The $Br/Cl \times 10^3$ varies from 3.7 to 4.8, and $I/Cl \times 10^6$ from 12 in vein quartz to 66 in greisen with fluorite. The charge balance (Q^+/Q^-) of the quartz sample from the hydrothermal vein is equal to 1. The Q^+/Q^- of the quartz from the greisen sample with fluorite is also relatively balanced, but the greisen sample with molybdenite has a charge balance of 2.3, which means that another not-analyzed anion must be present or either some solid phases enclosed in FI or a possibly present contaminating mineral phase dissolved during leachate preparation.

Table 6. Crush-leach analyses of fluid inclusions in quartz from Krupka (values in ppb).

Sample	**KR-11 (Greisen)**	**KR-12 (Greisen)**	**KR-12 (Vein)**
Li^+	27	30	32
Na^+	4496	4250	4055
K^+	2582	2124	1677
Mg^{2+}	602	173	94
Ca^{2+}	10,198	1878	952
F^-	81	219	250
Cl^-	9866	9179	8564
Br^-	47	38	31
I^-	1.4	0.6	0.1
NO_3^-	3829	1573	845
SO_4^{2-}	777	186	191
$Br/Cl \times 10^3$	4.8	4.2	3.7
Na/Br	95	111	129
$I/Cl \times 10^6$	15	66	12
Na/K	1.7	2.0	2.4
K/Na	0.6	0.5	0.4
Cl/SO_4	13	49	45
Q^+/Q^-	2.3	1.2	1.0

4.6. Hydrogen Isotopes

The δD values and water contents were determined for two mica samples (KR-5 and KR-7) and two clay minerals (KR-4 and KR-8). Greisen samples with different mineral compositions (see Table 1) and degrees of autometamorphism from the Knötel deposit were chosen so that the hydrogen isotope analyses covered both the greisenization and post-greisenization stages. A wide range of δD values was found, ranging between −54.6 and 33.6‰ V-SMOW (Table 7).

Table 7. The determined $\delta D_{mineral}$ values, contents of water and calculated δD_{fluid} for given temperatures in clay minerals and micas.

Mineral	Sample	$\delta D_{mineral}$ (‰ V-SMOW)	δD_{fluid} (‰ V-SMOW)	Temperature (°C)	Content of Water (%)
Dickite	KR-4	−22.2	−45.7 to −37.9	100–250	9.79
Dickite	KR-8	−51.2	−74.7 to −66.9	100–250	14.31
Phengite/Li-phengite	KR-7	−54.6	−92.4 to −77.8	350–400	2.34
Protolithionite/zinnwaldite	KR-5	33.6	−20.6 to −6.0	350–450	0.92

5. Discussion

5.1. Chemical Composition of Fluids

As is evident from microthermometric measurements, two fluid systems were involved in the formation of greisenized granites, greisens, and associated Sn-W hydrothermal veins in the Krupka ore district. The H_2O-salt fluid system is most frequent and occurs in all samples, all minerals, and all genetic types of inclusions of studied rocks and veins. Microthermometric data from fluid inclusions with the H_2O-salts fluid system were compared with already published data from other localities within the Czech and German parts of the Bohemian Massif. The data for the primary inclusions are very similar to the data from the Hub Stock [17] and Zinnwald [54], but the above-mentioned papers report a narrower range of homogenization temperatures than cover our data from Krupka (Figure 12). The melting temperature of the last ice crystal is in the range of −5 to 0 °C at all compared localities. The last crystal of ice in secondary inclusions from Krupka containing salt crystals melts at lower temperatures (down to −31 °C). The measured positive temperatures of melting of hydrohalite (2–5 °C) indicate metastable behavior [55]. Ref. [17] also reported high-salinity secondary inclusions in topaz and cassiterite from the Hub Stock, but most of these inclusions displayed metastable behavior during cooling runs. The mentioned paper reported the dissolution temperature of halite in inclusions in topaz in the range of 176–215 °C. All these inclusions homogenize to a liquid at temperatures of 468–512 °C. Multiphase inclusions in cassiterite homogenize into a liquid at temperatures of 485–498 °C, and halite in them dissolves at 158–167 °C [17]. Ref. [15] describes inclusions with solid phases in quartz from Krupka and in topaz from Cínovec but reported the salinity (35 wt. % NaCl eq.) from only a single inclusion containing crystals of salt. The above-mentioned paper also published the dissolution temperature of halite in the range 200–315 °C, whereas halite in inclusions measured in this work dissolves at temperatures between 120 and 335 °C (Figure 9). In a number of cases, the halite dissolves first and then disappears the vapor bubble, but in a few cases, halite dissolves after the bubble disappearance.

Less frequent is the H_2O-gases-salt fluid system, where a variable amount of CO_2 and trace amounts of N_2 and CH_4 were identified by microthermometric measurements (Section 4.3) and by Raman spectroscopy (Section 4.4). The non-aqueous phase is dominated by CO_2 in most cases, but in one case, pure CH_4 was found. Clathrate-bearing inclusions have low salinity (0–4.1 wt. % NaCl eq.; [40,41]). Compared to other localities with Sn-W or W mineralization, the non-aqueous phase in the fluid inclusions from Krupka shows a wider compositional range compared to the W mineralization from Tanvald granite from Jablonec nad Nisou [56], where CO_2 is always the dominant phase, and fluids have similar salinities (0–4.6 wt. % NaCl eq.). Carbon dioxide also dominates in the vapor phase from Cínovec ([57], unpublished data of authors) (Figure 13). The composition of the non-aqueous phase in the fluid inclusions suggests two possible trends, although the amount of data is small. One of these trends is already considered in [56] for W mineralization in Tanvald granite. In the primary inclusions from Krupka and from other Sn-W and W localities in the Bohemian Massif, a CO_2-rich fluid is probably mixed with fluids with very similar CH_4:N_2 ratios. The second trend for PSFI/SFI from Krupka seems to be characterized by a mixing of CO_2-rich fluids and CH_4-rich fluids with negligible N_2 contents (Figure 13). CH_4 in the fluids is a sign of a more reducing environment when the

fluids are captured. The contents of other gases (CH_4 and N_2) in addition to CO_2 were neglected during calculations of bulk fluid composition since the contents of those gases are very low or zero in PFI inclusions studied by Raman spectroscopy. Compositions and molar volumes of representative clathrate-bearing inclusions are listed in Table 8. The bulk molar volume of fluids in FI with volatiles ranges from 37.3 to 84.9 cm^3/mol, while the highest values are reached in quartz from greisen in sample KR-12 (Table 9). The calculated amount of CO_2 in inclusions ranges from 2.6 to 16.5 mol. % (Table 9).

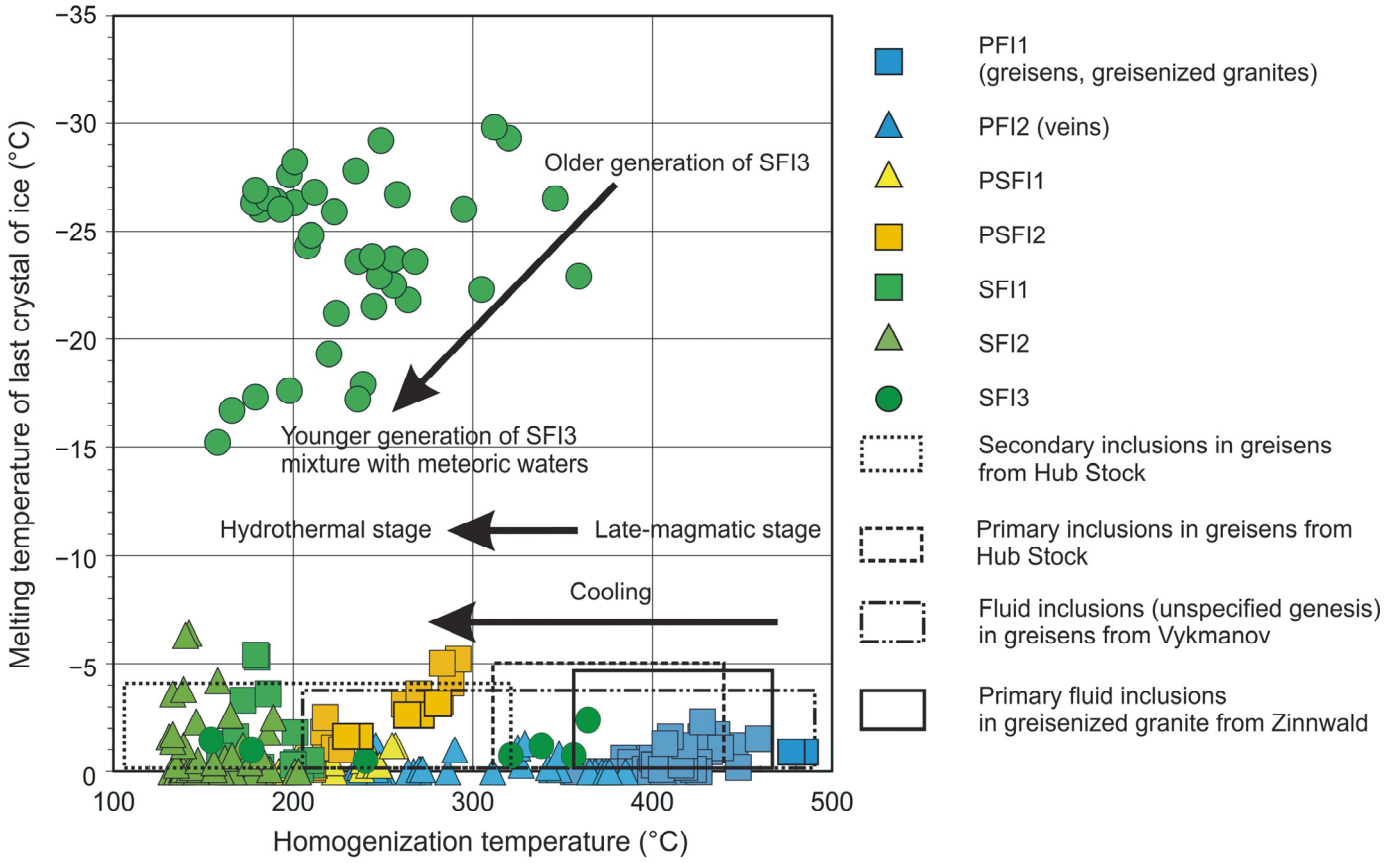


Figure 12. Plot of temperature of homogenization vs. ice melting temperature for fluid inclusions from Krupka and comparison with localities Vykmanov [16], Horní Slavkov–Hub Stock [17], and Zinnwald [54].

Table 8. Composition and molar volumes of representative clathrate-bearing inclusions from the Krupka ore district.

Sample	KNM-2	KMN-2	KNM-2	KNM-1	KR-5	KR-12
Mineral	Tpz	Tpz	Qtz	Qtz	Cst	Qtz
Genesis	PFI1	PFI1	PFI1	PFI1	PFI1	PFI1
Th_v (°C)	408	403	412	422	396	392
Tm_{ice} (°C)	−0.2	−0.1	−0.7	−0.8	−0.2	−2.1
Tm_{cla} (°C)	4.6	6.1	5.1	5.8	5.6	4.2
LVR	0.2	0.3	0.2	0.4	0.3	0.2
$X(H_2O)$	0.89	0.90	0.87	0.91	0.90	0.88
$X(CO_2)$	0.11	0.09	0.10	0.07	0.08	0.10
X(NaCl)	0.00	0.01	0.02	0.02	0.02	0.02
Molar volume (cm^3/mol)	83.0	56.8	79.5	42.9	58.5	82.5

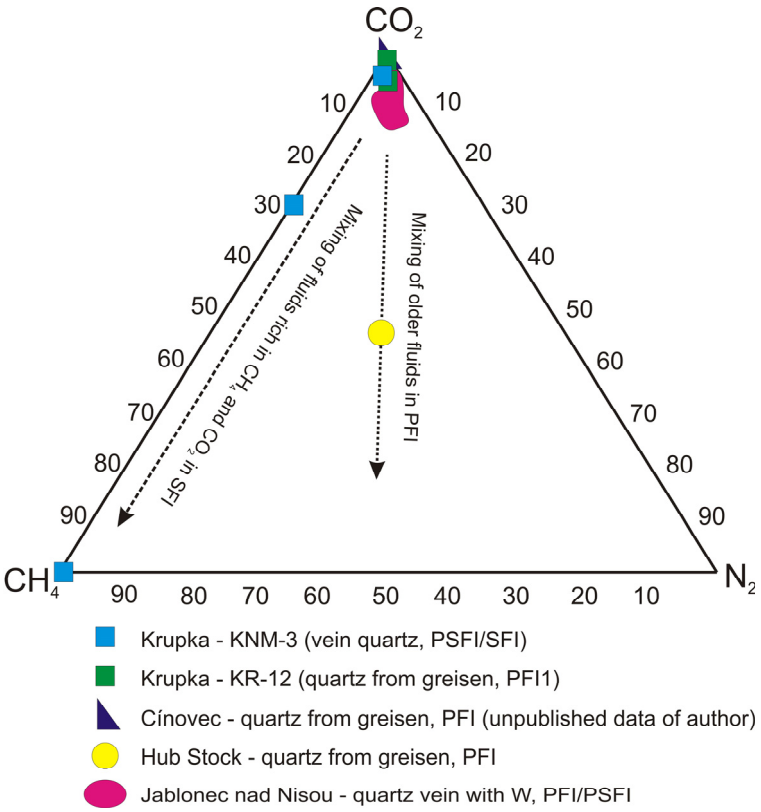


Figure 13. Results of Raman analyses of non-aqueous phases of fluid inclusions from Krupka in ternary plot CO_2-CH_4-N_2 and comparison with samples from other localities in the Bohemian Massif, W-mineralization from Jablonec nad Nisou [56] and greisens from Hub Stock [17].

Table 9. Ranges of composition and molar volumes of clathrate-bearing fluid inclusions from the Krupka ore district.

Sample	Mineral	Genesis	Salinity (wt. % NaCl eq.)	Molar Volume (cm^3/mol)	mol. % CO_2
PRK-1	Cst	PFI1/PSFI1	0.0–2.8	79.3–83.4	12.6–14.6
KR-5	Cst	PFI1	3.1–4.0	56.4–55.8	8.1–9.4
KR-12	Qtz	PFI1	3.2–3.4	81.6–84.9	10.7–11.3
KNM-1	Qtz	PFI1	1.3–3.3	55.9–81.7	2.6–8.9
KNM-2	Qtz	PFI1	1.5–3.9	58.6–81.6	7.7–14.8
KNM-2	Tpz	PFI1	0.5–4.1	56.6–80.2	7.6–16.5

5.2. P-T Conditions of Greisenization and Post-Greisenization Processes

Considering the facts that the primary inclusions with and also without CO_2 in some samples of greisens homogenize in three different modes (to vapor, to liquid, and in a critical way) and the homogenization temperatures differ only slightly, it is likely that these inclusions were trapped from a heterogeneous fluid [49]. In such a situation, the minimum recorded homogenization temperatures would correspond to the actual temperatures of fluid entrapment. For vapor-homogenizing inclusions, it was possible to calculate the pressure at the time of fluid entrapment. The results even with bulk molar volume and mol. % of CO_2 in representative fluid inclusions are summarized in Table 10, and results of P-T calculations are visualized in Figure 14. The results show that the greisenization process took place at temperatures of 370 to 490 °C at low pressures from 155 to 371 bar. The fluids with CO_2 were trapped at higher pressures (322 to 371 bar) than fluids of system H_2O-NaCl. Fluids without volatile components were captured at pressures of 155–320 bar, with the highest pressures calculated for inclusions in quartz from greisens from samples KR-11 and KR-12. The pressure and temperature conditions of greisenization given from the Hub

Stock [17] correspond to temperatures of 350 to 450 °C and 250 to 530 bar. Greisenization in the western part of the Erzgebirge took place in a wider temperature and pressure interval (Figure 14).

Table 10. Calculated bulk molar volumes of vapor-homogenizing fluid inclusions trapped from heterogenous fluid and calculated pressure of their entrapment.

Fluid System	**H_2O-CO_2-(NaCl)**		**H_2O-NaCl**					
Sample Mineral	**KNM-2 tpz**	**KR-12 qtz**	**PRK-1 qtz**	**PRK-1 tpz**	**KR-3 qtz**	**KNM-2 tpz**	**KR-11 qtz**	**KR-12 qtz**
Th_v (°C)	403, 408	392	392–425	408–456	398–431	405–416	379–428	381–456
Tm_{ice} (°C)	−0.1,−0.2	−2.1	−2.3 to −0.2	−0.3 to −0.1	−2.1 to −0.3	−0.4 to 0	−0.5 to 0	−2.1 to −0.2
Tm_{cla} (°C)	4.6, 6.1	4.2						
LVR	0.2, 0.3	0.2	0.2–0.4	0.2–0.3	0.2–0.3	0.2–0.3	0.1–0.3	0.1–0.4
Mol. % CO_2	10.7, 8.9	9.8						
Bulk molar volume (cm^3/mol)	56.8, 83.0	82.4	38.3–46.7	47.0–95.1	39.0–52.9	45.2–52.2	37.5–60.2	33.7–80.54
Pressure (bar)	352, 371	322	173–223	197–268	182–224	193–209	155–320	157–313

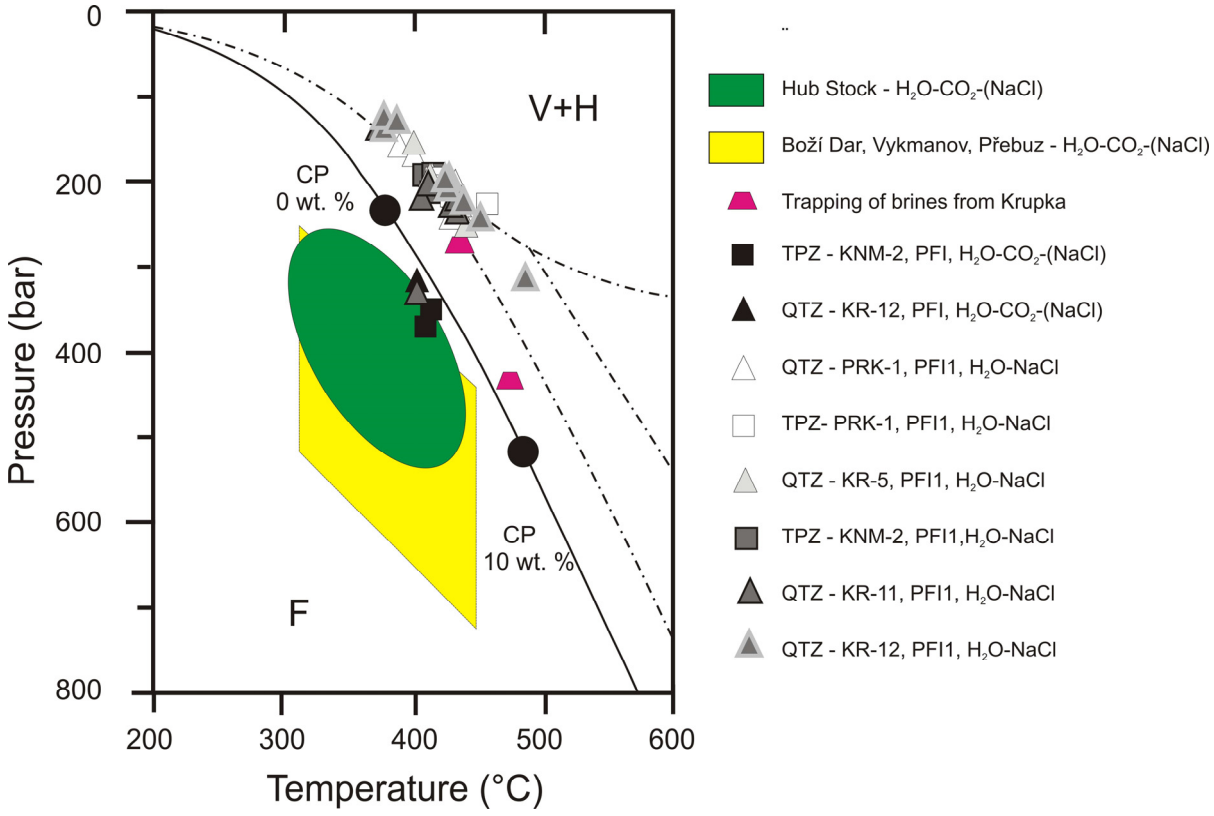


Figure 14. Pressure and temperature conditions of trapping of PFI connected with process of greisenization from Krupka and comparison with other localities, Horní Slavkov–Hub Stock [17], Boží Dar, Vykmanov, Přebuz [16] and trapping of brines from Krupka [15]. Diagram modified after [58].

In the vast majority, PSFI1,2 and SFI1,2 homogenize only to liquid, and conditions of capture of such homogeneous fluid cannot be determined in the absence of results from independent geothermometers or geobarometers. The post-greisenization stage, characterized by the formation of hydrothermal veins with fluorite, clay minerals (dickite, illite), and Fe oxides and oxyhydroxides, took place at low temperatures because secondary fluid inclusions that contain only a liquid phase indicate the capture of fluid inclusions at temperatures less than 100 °C [49]. However, the temperature values of the fluids captured by PSFI1, SFI1, and SFI3 will be much higher, as shown by the measured homogenization

temperatures reaching up to 370 °C. Hence, the available data from these late fluid inclusions likely cover the whole cooling history of the host magmatic rock. Ref. [15] reports the temperature and pressure conditions for two episodes of trapping of high-salinity fluids in quartz from Krupka (Figure 14) and states values of 430–440 °C and 280 bar and 480–490 °C and 460 bar.

5.3. Origin of Fluids

As in the fluids from the Hub Stock [17], sodium chloride dominates in the fluids from Krupka according to the recorded eutectic temperatures of the fluid inclusions [59]. Mg and Fe chlorides are likely present, depending on the lower values of the eutectic temperatures (see Section 4.3), in addition to NaCl in some secondary inclusions. The leachates of fluid inclusions showed the presence of nitrates and sulfates in relatively significant amounts in addition to chlorides (see Table 3). Sulfates are present as part of the brines in SFI3, as verified by Raman spectroscopy. Nitrates can be leached from overlying sedimentary rocks or basins and infiltrated along fractures into the granitoid massif. Among the cations, Na^+ usually dominates, but in one sample of quartz from greisen from the Prokop Stock, calcium is predominant. The high content of Ca in fluids can be explained by the albitization of plagioclase when the rock is depleted of Ca, which can then be present in greisenizing solutions [60]. Another explanation may be the dissolution of calcite that is present as a solid in SFI3 inclusions. Calcium-rich fluid was also found in topaz and cassiterite from the Hub Stock [17] (Figure 15). The I/Cl values (12, 15, and 66 × 10^{-6}; Table 3) and Br/Cl (3.7, 4.2 and 4.8 × 10^{-3}) in fluids from Krupka are comparable with shield brines from the Canadian and Baltic Shields and also fall into the field of post-Variscan high-salinity fluids of the Bohemian Massif (Figure 16). The charge balance (Q^+/Q^-) of one greisen sample from Krupka is not balanced (Table 3) and indicates the presence of other anions in the fluids. The presence of carbonates in fluids seems to be the most probable, as calcite and siderite solids were determined in fluid inclusions by means of Raman spectroscopy (Figure 11). The Na/K in fluids from Knötel–Prokop Stock is higher than in fluids from Martin adit referred by [15]. This is very likely caused by a higher degree of argillitization of samples from Prokop Stock. As stated [61,62], the argillitization process begins around 200 °C and is associated with the activity of low-salinity and acid solutions poor in sulfate ions.

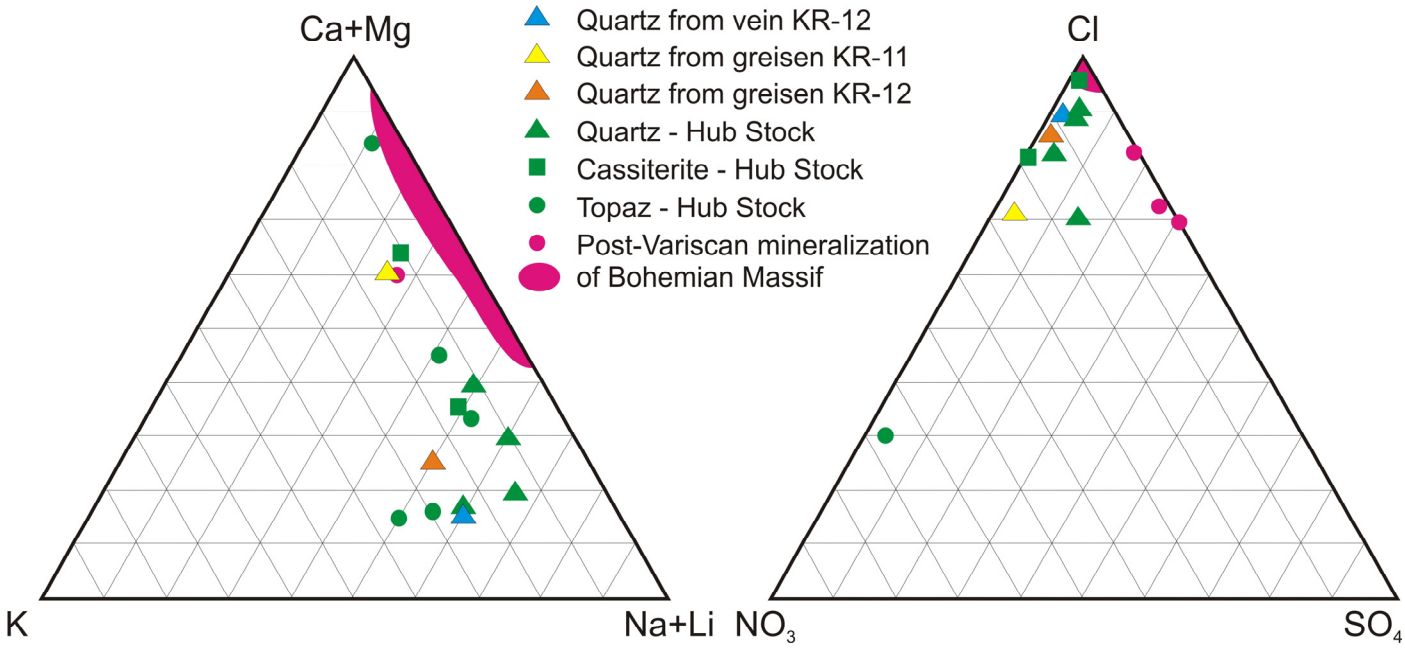


Figure 15. Ternary diagrams NO_3^--SO_4^{2-}-Cl^- and K^+-(Na^++Li^+)-(Ca^{2+}+Mg^{2+}) in leachates of fluid inclusions from Krupka and comparison with leachates from Horní Slavkov–Hub Stock [17] and post-Variscan hydrothermal mineralization from the Bohemian Massif [63].

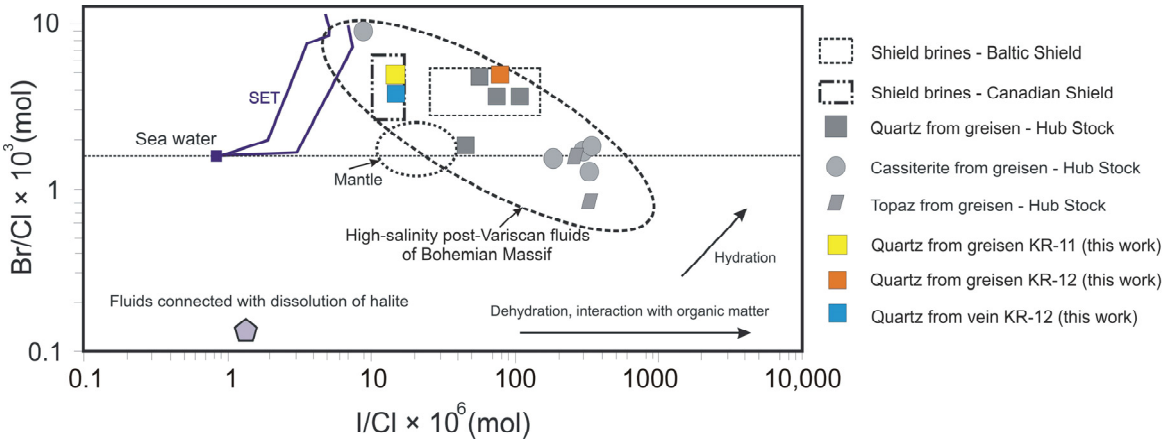


Figure 16. I/Cl vs. Br/Cl plot for leachates of fluid inclusions from Krupka and comparison with other localities—Hub Stock [17], high-salinity post-Variscan fluids of Bohemian Massif [63,64] and various other sources—sea water, mantle; SET—seawater evaporation trajectory. Plot modified after [17].

High-salinity PSFI/SFI3 are probably connected with fluids derived from brines during the secondary boiling of magma. When the magma is initially enriched in CO_2 and other volatile components, fluids with different compositions can be exsolved during the secondary boiling [65]. Refs. [54,66,67] deal with the research of fluid and melt inclusions in altered granites, greisens, and associated hydrothermal veins from the German part of Erzgebirge. According to these studies, granitic melt at great depths and at high temperatures is undersaturated with H_2O. During melt-fluid separation at the interface of the magmatic and hydrothermal phases, high-temperature brines are often exsolved, which can concentrate metals and produce economically important deposits. In the case of the Krupka ore district, high-salinity fluids and low-salinity steam were also exsolved. Some solid phases (quartz and sulfides) occurring in the high-salinity fluid inclusions do not dissolve even at high temperatures. As already mentioned above, multiphase inclusions probably belong to at least two generations, but they do not differ in principle either in terms of homogenization temperature. However, in some inclusions (apparently in the younger generation), there is a decrease in salinity, probably due to interaction with meteoric waters. Very low salinities have multiphase inclusions without salts, containing only captured crystals of other mineral phases (mainly topaz and quartz). Evidence of brines in greisens is also known from other localities in the Bohemian Massif, including the Hub Stock near Horní Slavkov, Krupka, and Cínovec [15,17].

Some clues on the origin of the fluids also offer analyses of stable isotopes of hydrogen in micas and clay minerals. According to δD_{fluid} values ranging between −92.4 and −6.0‰ V-SMOW, calculated from $\delta D_{mineral}$ values and estimated formation temperatures (Table 7), the fluids were most likely derived from a magmatic source, but some contribution of another source (sedimentary or metamorphic fluid) cannot be excluded (Figure 17). The calculated δD values of greisenizing fluids (sample KR-7) approximately correspond with the results from other localities in Bohemian Massif and other world Sn-W deposits (Figure 17). The δD_{fluid} for protolithionite/zinnwaldite from greisen sample KR-5 has only a slightly negative value, which can be the consequence of the redistribution of isotopes during phase separation associated with boiling [68] of greisenizing fluids. Samples KR-4 and KR-8 originated from strongly altered greisens with fluorite and clay minerals. The δD_{fluid} values of these samples most likely correspond to an origin in meteoric waters. The δD_{fluid} values for samples KR-4 and KR-5 are very similar to the δD values of altered granites from the Bohemian Massif (Figure 17). Based on oxygen isotopes, the participation of both magmatic and meteoric fluids during the formation of quartz veins with Sn-W mineralization was also reported [69] from the Takatori deposit in Japan.

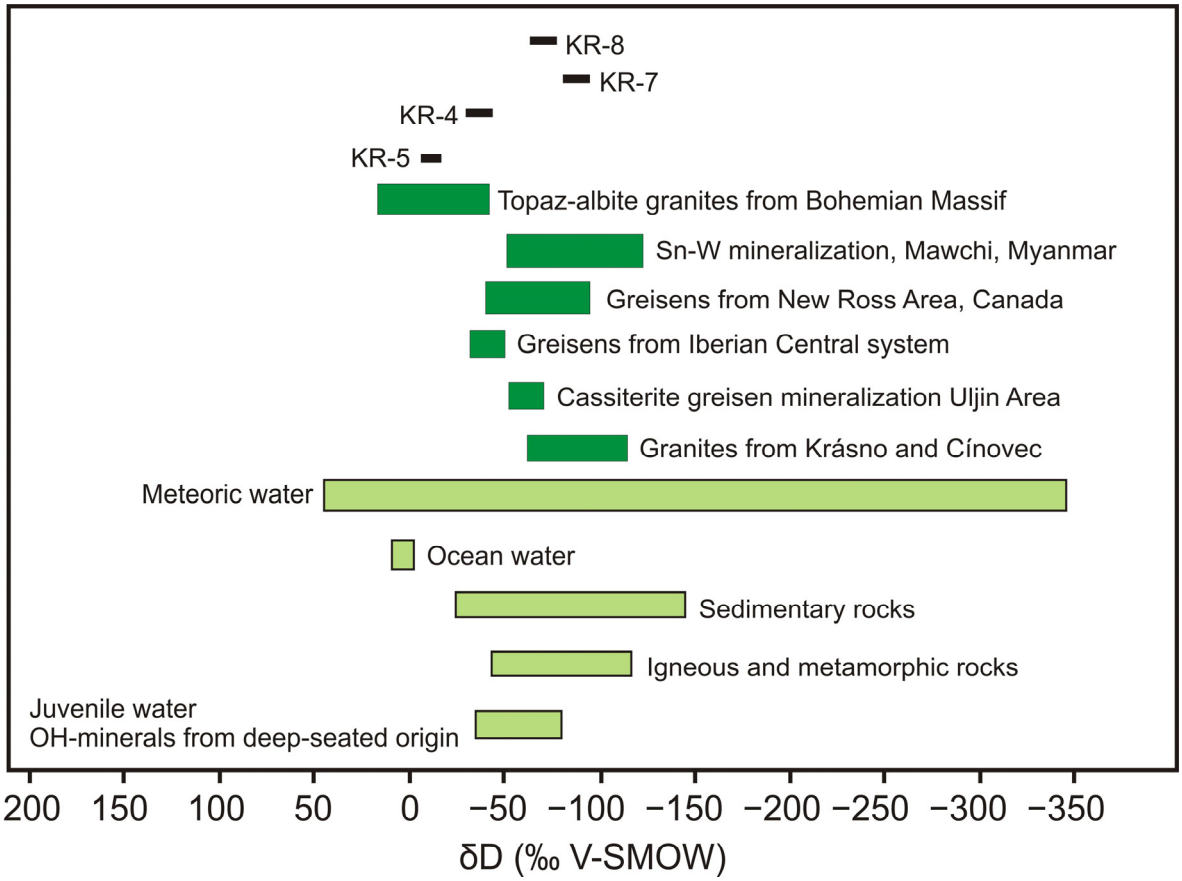


Figure 17. The calculated δD values of parent fluids from samples from Krupka ore district and their comparison with geologically important reservoirs [68], granites from Horní Slavkov–Hub Stock [17] and Cínovec [14], greisens from Iberian Central system [70], greisen cassiterite mineralization from Uljin Area [71], greisens from New Ross area in Canada [72], Sn-W mineralization, Mawchi, Myanmar [73], and unpublished data by M. René for topaz-albite granites of the Bohemian Massif.

Low salinity and the presence of only single-phase secondary inclusions in a number of greisen and vein samples suggest that the hydrothermal stage was associated with meteoric waters that infiltrated the hydrothermal system [48].

Based on the evidence obtained in this work, it is possible to construct a simplified model of fluid evolution. Figure 18 illustrates the evolution of fluids in the Knötel area. The initial stages of the greisenization of granites involved H_2O-NaCl-gas (CO_2, CH_4, and N_2) fluids with low salinity. As the temperature decreased and the magma rose closer to the surface, the exsolution of high-salinity fluids (up to 31 wt. % NaCl eq.) occurred, which are trapped in multiphase inclusions interpreted as PSFI or as an older generation of SFI3. These late inclusions have a relatively low degree of filling. Further cooling led to the infiltration of external fluids originating in either meteoric water or overlying sedimentary rocks or sedimentary basins. These fluids had low salinity and often healed cracks in greisens and hydrothermal veins. The degree of filling of FI is still relatively low. In the same stage of evolution, multiphase inclusions could also have been trapped, which represent a mix of magmatogenic brines and fluids originating from meteoric waters. The salinity of fluids trapped in SFI3 inclusions of the younger generation is slightly lower than that of fluids of the older generation. In the final stages of the hydrothermal stage, only low-salinity, low-temperature fluids dominated by surface waters healed fractures in greisens and newly formed veins (Figure 18).

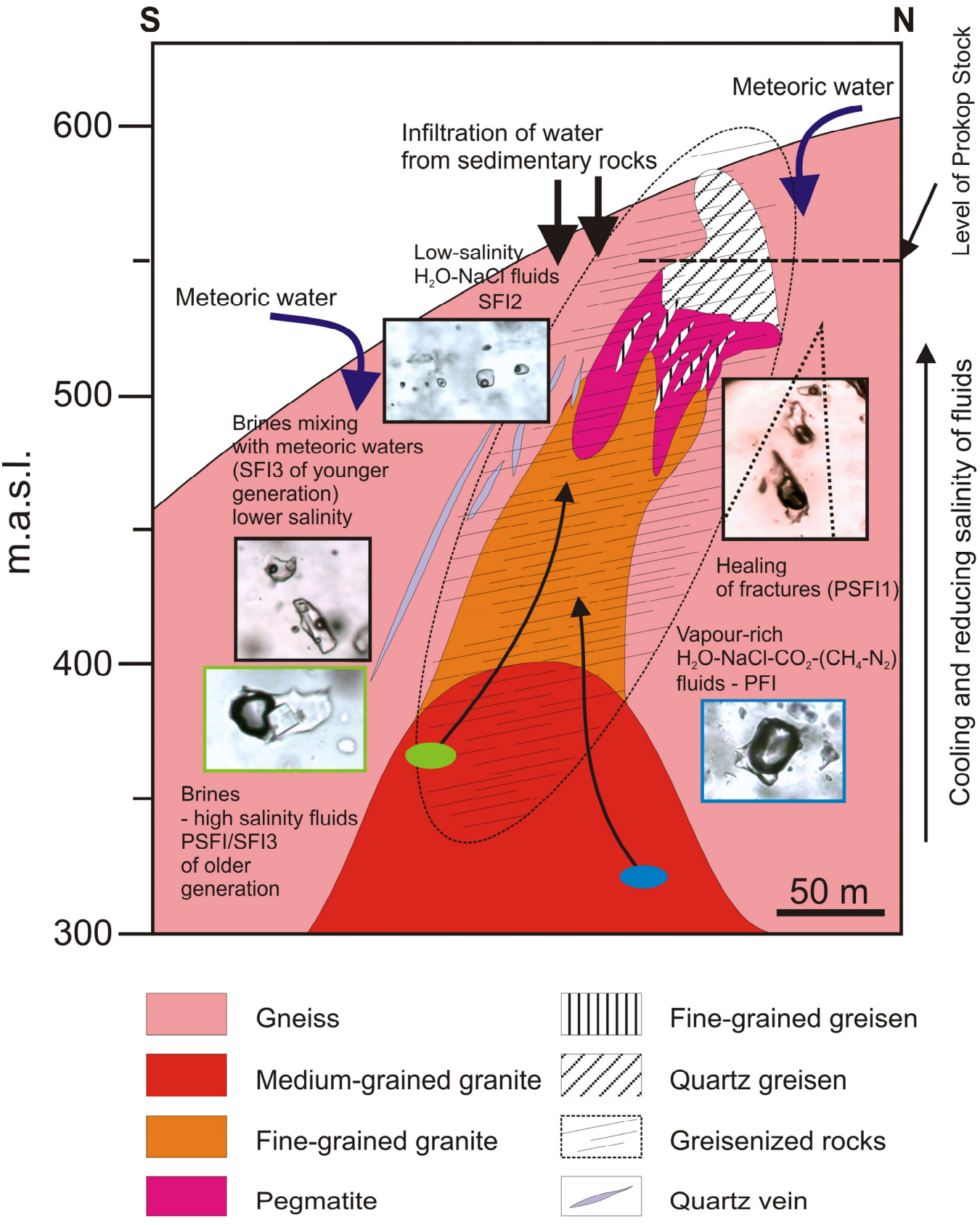


Figure 18. Simplified model of fluid evolution in the Knötel Stock.

6. Conclusions

The results of the study of greisenized granites, greisens, and associated hydrothermal veins from the Krupka ore district showed that the greisenization process took place at temperatures of 370–490 °C and pressures of 155–371 bar. The greisenization process was related to the activity of near-critical low-salinity aqueous fluids with low gas content (CO_2, N_2, CH_4). The post-greisenization processes, including the formation of some ore veins and the crystallization of clay and other secondary minerals, were associated with the activity of low-salinity and high-salinity fluids with temperatures of <120–370 °C and containing captured or daughter crystals, predominantly of salts and carbonates. According to the isotopic composition of H of fluids, the source of fluids is partly magmatogenic, but post-greisenizing fluids also originated in meteoric waters and fluids derived from sedimentary rocks.

Author Contributions: Conceptualization, M.K.K., Z.D., M.R., W.P., J.U., J.K., and K.K.; methodology, M.K.K., Z.D., V.M., J.U., and J.K.; investigation, M.K.K. and Z.D.; resources, M.K.K.; writing—original draft preparation, M.K.K.; writing—review and editing, M.K.K., Z.D., M.R., W.P., J.U., J.K., and K.K. All authors have read and agreed to the published version of the manuscript.

Funding: The study was financially supported by the Ministry of Culture of the Czech Republic (long-term project DKRVO 2024-2028/1.I.a; National Museum, 00023272) to Z.D. and J.U, DKRVO, long-term conceptual development of a research organization Research Institute for Building Materials project 2023–2027 and EXPRO 2019 project of the Czech Science Foundation (No. 19-29124X) to M.K.K.

Data Availability Statement: All data are contained in this paper.

Acknowledgments: H. Taubald (University of Tübingen) is thanked for analyses of hydrogen isotopes. Constructive comments by two referees helped to improve the original draft of the manuscript.

Conflicts of Interest: The authors declare no conflicts of interest. The funder had no role in the design of this study, in the collection, analysis, or interpretation of data, in the writing of this manuscript, or in the decision to publish these results.

References

1. Lange, H.; Tischendorf, G.; Palchen, W.; Klemm, I.; Ossenkopf, W. Zur Petrographie und Geochemie der Granite des Erzgebirges. *Geologie* **1972**, *21*, 457–494.
2. Teuscher, E.O. Primäre Bildungen des granitischen Magmas und seine Restlösungen im Massif von Eibenstock-Neudeck. *Miner. Petr. Mitt.* **1936**, *19*, 211–266.
3. Beus, A.A.; Zalashkova, N.E. High-temperature postmagmatic metasomatic processes in grantioids. *Izv. Akad. Nauk. SSSR Ser. Geol.* **1962**, *4*, 13–31.
4. Štemprok, M. Petrology and the vertical extent of mineralization in the Cínovec (Zinnwald) granite cupola. *Sbor. Geol. Věd Lož. Geol. Miner.* **1965**, *5*, 7–106.
5. Tischendorf, G.; Förster, H.J. Hercynian granite magmatism and related metallogenesis in the Erzgebirge. *Monogr. Ser. Miner. Depos.* **1994**, *31*, 5–23.
6. Kovalenko, V. *Petrology and Geochemistry of Rare Metal Granites*; Nauka: Novosibirsk, Russia, 1977; p. 206.
7. Černý, P.; Blevin, P.L.; Cuney, M.; London, D. Granite-Related Ore Deposits. *Econ. Geol.* **2006**, *107*, 337–370. [CrossRef]
8. Jarchovský, T.; Pavlů, D. Albite-topaz microgranite from Horní Slavkov (Slavkovský les Mts.) NW Bohemia. *Věst. Ústř. Úst. Geol.* **1991**, *66*, 13–22. [CrossRef]
9. Eisenreich, M.; Breiter, K. Krupka Sn-W-Mo deposits in Eastern Krušné hory Mts. *Věst. Čes. Geol. Úst.* **1993**, *63*, 3.
10. Breiter, K. From explosive breccia to unidirectional solidification textures: Magmatic evolution of a phosphorus- and fluorine-rich granite system (Podlesí, Krušné hory Mts., Czech Republic). *Bull. Geosci.* **2002**, *77*, 67–92.
11. René, M.; Škoda, R. Nb-Ta-Ti oxides fractionation in rare-metal granites: Krásno-Horní Slavkov ore district, Czech Republic. *Miner. Petrol.* **2011**, *103*, 37–48. [CrossRef]
12. Thomas, R. Estimation of the viscosity and the water content of silicate melts from melt inclusion data. *Eur. J. Miner.* **1994**, *6*, 511–535. [CrossRef]
13. Jarchovský, T. The nature and genesis of greisen stock at Krásno, Slavkovský les area—Western Bohemia, Czech Republic. *J. Czech Geol. Soc.* **2006**, *51*, 201–216. [CrossRef]
14. Dolejš, D.; Štemprok, M. Magmatic and hydrothermal evolution of Li-F granites: Cínovec and Krásno intrusions, Krušné hory batholith, Czech Republic. *Bull. Geosci.* **2001**, *76*, 77–79.

15. Ďurišová, J.; Charoy, B.; Weisbrod, A. Fluid inclusion studies in minerals from tin and tungsten deposits in the Krušné Hory Mountains (Czechoslovakia). *Bull. Minéral.* **1979**, *102*, 665–675. [CrossRef]
16. Ďurišová, J. Formation conditions of greisen parageneses of the western Erzgebirge Mountains. *Věst. Ústř. Úst. Geol.* **1984**, *59*, 141–152. (In Czech)
17. Dolníček, Z.; René, M.; Prochaska, W.; Kovář, M. Fluid evolution of the Hub Stock, Horní Slavkov–Krásno Sn–W ore district, Bohemian Massif, Czech Republic. *Miner. Depos.* **2012**, *47*, 821–833. [CrossRef]
18. Štemprok, M.; Pivec, E.; Langrová, A. The petrogenesis of a wolframite-bearing greisen in the Vykmanov granite stock, Western Krušné hory pluton (Czech Republic). *Bull. Geosci.* **2005**, *80*, 165–184.
19. Matte, P.; Maluski, H.; Rajlich, P.; Franke, W. Terrane boundaries in the Bohemian Massif: Result of large-scale Variscan shearing. *Tectonophysics* **1990**, *177*, 151–170. [CrossRef]
20. Klomínský, J.; Jarchovský, T.; Rajpot, G.S. *Atlas of Plutonic Rocks and Orthogneisses in the Bohemian Massif, Saxothuringicum*; Czech Geological Survey: Prague, Czech Republic, 2010; p. 94.
21. Sejkora, J.; Breiter, K. Historical Krupka ore district, Erzgebirge Mountains. *Bull. Miner. Petrol. Odd. Nár. Muz.* **1999**, *7*, 29. (In Czech)
22. Janečka, J.; Malásek, F.; Štemprok, M.; Tischendorf, G.; Zoubek, V. *Metallogeny of Tin and Tungsten in the Krušné Hory—Erzgebirge*; International Geological Correlation Programme—Excursion Guide; Ústřední Ústav Geologický: Prague, Czech Republic, 1974.
23. Schumacher, F. Die Erzgebirgishe Metallprovinz und ihre Genesis. *Erzmetall* **1933**, *30*, 161–166.
24. Watznauer, A. Die erzgebirgischen Granitintrusionen. *Geologie* **1954**, *6–7*, 688–706.
25. Breiter, K.; Förster, H.-J.; Seltmann, R. Variscan silicic magmatism and related tin-tungsten mineralization in the Erzgebirge-Slavkovský les metallogenic province. *Miner. Depos.* **1999**, *34*, 505–521. [CrossRef]
26. Forster, H.-J.; Tischendorf, G.; Trumbull, R.B.; Gottesmann, B. Late-Collisional Granites in the Variscan Erzgebirge, Germany. *J. Pet.* **1999**, *40*, 1613–1645. [CrossRef]
27. Škvor, V. *Geology of the Czech Part of the Erzgebirge Mountains and Smrčiny*; Ústřední Ústav Geologický: Prague, Czech Republic, 1975; p. 48. (In Czech)
28. Škvor, V. The Krušné Hory Mountains pluton and its interpretation. *Věst. Ústř. Úst. Geol.* **1986**, *61*, 65–71. (In Czech)
29. Siebel, W.; Trzebski, R.; Stettner, G.; Hecht, L.; Casten, U.; Höhndorf, A.; Műller, P. Granitoid magmatism of the NW Bohemian massif revealed: Gravity data, composition, age relations and phase concept. *Geol. Rund.* **1997**, *86*, 545–563. [CrossRef]
30. Romer, R.L.; Thomas, R.; Stein, H.J.; Rhede, D. Dating multiply overprinted Sn-mineralized granites—Examples from the Erzgebirge, Germany. *Miner. Depos.* **2007**, *42*, 337–359. [CrossRef]
31. Tichomirova, M.; Leonhardt, D. New age determination (Pb/Pb zircon evaporation, Rb/Sr) on the granites from Aus-Schwarzenberg and Eibenstock, Western Erzgebirge, Germany. *Z. Geol. Wiss.* **2010**, *38*, 99–123.
32. Štemprok, M.; Blecha, V. Variscan Sn–W–Mo metallogeny in the gravity picture of the Krušné hory/Erzgebirge granite batholith (Central Europe). *Ore Geol. Rev.* **2015**, *69*, 285–300. [CrossRef]
33. Richter, P.; Stettner, G. Geochemische und petrographishe Untersuchungen der Fichtelgebirgsgranite. *Geologica Bavar.* **1979**, *78*, 144.
34. Štemprok, M.; Šulcek, Z. Geochemical profile through an ore-bearing lithium granite. *Econ. Geol.* **1969**, *64*, 392–404. [CrossRef]
35. Peterková, T.; Dolejš, D. Magmatic-hydrothermal evolution of highly evolved granite stock Knöttel near Krupka in Erzgebirge. *Zpr. Geol. Výzk.* **2017**, *50*, 189–194. [CrossRef]
36. Peterková, T.; Dolejš, D. Magmatic-hydrothermal transition of Mo-W-mineralized granite-pegmatite-greisen system recorded by trace elements in quartz: Krupka district, Eastern Krušné hory/Erzgebirge. *Chem. Geol.* **2019**, *523*, 179–202. [CrossRef]
37. Žák, L. Origin of the molybdenite and feldspar deposit of Krupka. II. Paragenetic relations. *Acta Univ. Carol. Geol.* **1966**, *22*, 167–195.
38. Bodnar, R. Revised equation and table for determining the freezing point depression of H_2O-NaCl solutions. *Geochim. Cosmochim. Acta* **1993**, *57*, 683–684. [CrossRef]
39. Duan, Z.; Møller, N.; Weare, J.H. An equation of state for the CH_4-CO_2-H_2O system: I. Pure systems from 0 to 1000 °C and 0 to 8000 bar. *Geochim. Cosmochim. Acta* **1992**, *56*, 2605–2617. [CrossRef]
40. Duan, Z.; Møller, N.; Weare, J.H. An equation of state for the CH_4-CO_2-H_2O system: II. Mixtures from 50 to 1000 °C and 0 to 1000 bar. *Geochim. Cosmochim. Acta* **1992**, *56*, 2619–2631. [CrossRef]
41. Bowers, T.S.; Helgeson, H.C. Calculation of the thermodynamic and geochemical consequences of nonideal mixing in the system H_2O-CO_2-NaCl fluids at high pressures and temperatures. *Geochim. Cosmochim. Acta* **1983**, *47*, 1247–1275. [CrossRef]
42. Zhang, Y.-G.; Frantz, J.D. Determination of the homogenization temperatures and densities of supercritical fluids in the system NaCl–KCl–$CaCl_2$–H_2O using synthetic fluid inclusions. *Chem. Geol.* **1987**, *64*, 335–345. [CrossRef]
43. Bakker, R.J. Adaptation of the Bowers and Helgeson (1983) equation of state to the H_2O–CO_2–CH_4–N_2–NaCl system. *Chem. Geol.* **1999**, *154*, 225–236. [CrossRef]
44. Available online: https://fluids.unileoben.ac.at/Computer.html (accessed on 17 December 2023).
45. Bodnar, R.J.; Vityk, M.O. Interpretation of microthermometric data for H_2O-NaCl fluid inclusions. In *Fluid Inclusions in Minerals: Methods and Applications*; De Vivo, B., Frezzotii, M.L., Eds.; Short Course IMA: Pontignano-Siena, Italy, 1994; pp. 117–130.
46. Knight, C.; Bodnar, R. Synthetic fluid inclusions: IX. Critical PVTX properties of NaCl-H_2O solutions. *Geochim. Cosmochim. Acta* **1989**, *53*, 3–8. [CrossRef]
47. Frezzotti, M.L.; Tecce, F.; Casagli, A. Raman spectroscopy for fluid inclusion analysis. *J. Geochem. Explor.* **2012**, *112*, 1–20. [CrossRef]
48. Burke, E.A.J. Raman microspectrometry of fluid inclusions. *Lithos* **2001**, *55*, 139–158. [CrossRef]

49. Hurai, V.; Huraiová, M.; Slobodník, M.; Thomas, R. *Geofluids Development in Microthermometry, Spectroscopy, Thermodynamics, and Stable Isotopes*, 1st ed.; Elsevier Inc.: Amsterdam, The Netherlands, 2015. [CrossRef]
50. Vennemann, T.V.; O´Neil, J.R. A simple and inexpensive method of hydrogen isotope and water analyses of minerals and rocks based on zinc reagent. *Chem. Geol.* **1993**, *103*, 227–234. [CrossRef]
51. Suzuoki, T.; Epstein, S. Hydrogen isotope fractionation between OH-bearing minerals and water. *Geochim. Cosmochim. Acta* **1976**, *40*, 1229–1240. [CrossRef]
52. Gilg, H.A.; Sheppard, S.M. Hydrogen isotope fractionation between kaolinite and water revisited. *Geochim. Cosmochim. Acta* **1996**, *60*, 529–533. [CrossRef]
53. Lecumberri-Sanchez, P.; Steele-MacInnis, M.; Bodnar, R.J. A numerical model to estimate trapping conditions of fluid inclusions that homogenize by halite disappearance. *Geochim. Cosmochim. Acta* **2012**, *92*, 14–22. [CrossRef]
54. Webster, J.; Thomas, R.; Förster, H.J.; Seltman, R.; Tappen, C. Geochemical evolution of halogen-enriched granite magmas and mineralizing fluids of the Zinnwald tin-tungsten mining district, Erzgebirge, Germany. *Miner. Depos.* **2004**, *39*, 452–472. [CrossRef]
55. Zwart, E.W.; Touret, J.L.R. Melting behavior and composition of aqueous fluid inclusions on fluorite and calcite: Application within system H_2O-$CaCl_2$-NaCl. *Eur. J. Miner.* **1994**, *6*, 773–786. [CrossRef]
56. Ulmanová, J.; Dolníček, Z. New occurrence of vein W-mineralization in Tanvald granite from Jablonec nad Nisou—Mineralogy, chemical compositions of minerals and fluid inclusions. *Bull. Min. Petrolog.* **2019**, *27*, 193–204. (In Czech)
57. Nasdala, L.; Smith, D.C.; Kaindl, R.; Ziemann, M.A. Raman spectroscopy: Analytical perspectives in mineralogical research. *EMU Notes Miner.* **2004**, *6*, 20. [CrossRef]
58. Tsuruoka, S. The Evolution of Hydrothermal Fluids from the Deep Porphyry Environment to the Shallow Epithermal Environment. Ph.D. Thesis, Colorado School of Mines, Faculty and the Board of Trustees, Golden, CO, USA, 2017. Volume 197. p. 17.
59. Borisenko, A.S. Izučenije solevogo sostava rastvorov gazovožidkich vklučenij v mineralach metodom kriometrii. *Geolog. Geofiz.* **1977**, *8*, 16–27.
60. Klemm, W. Chemical evolution of hydrothermal solutions during Variscan and post-Variscan mineralization in Erzgebirge, Germany. In *Metallogeny of Collisional Orogens: Focused on the Erzgebirge and Comparable Metallogenic Settings*; Seltmann, R., Kämpf, H., Möller, P., Eds.; Czech Geological Survey: Prague, Czech Republic, 1994; pp. 150–158.
61. Charoy, B. Ploemeur kaolin deposit (Brittany), an example of hydrothermal alteration. *Pétrologie* **1975**, *1*, 253–266.
62. Charoy, B. *Definition of Importance des Phenomenes Deuteriques et des Fluids Associes dans les Granites. Consequences Metallogeniques*; Sciences de la Terre: Paris, France, 1979; p. 364.
63. Dolníček, Z.; Fojt, B.; Prochaska, W.; Kučera, J.; Sulovský, P. Origin of the Zálesí U–Ni–Co–As–Ag/Bi deposit, Bohemian Massif, Czech Republic: Fluid inclusion and stable isotope constraints. *Miner. Depos.* **2009**, *44*, 81–97. [CrossRef]
64. Kotlánová, M.; Dolníček, Z. Origin and chemical composition of fluids of post-Variscan hydrothermal mineralization at locality Zlatý důl near Hlubočky (Lower Carboniferous of the Nízký Jeseník Upland). *Geol. Výzk. Mor. Slez.* **2016**, *23*, 74–80. (In Czech) [CrossRef]
65. Edmonds, M.; Woods, A.W. Exsolved volatiles in magma reservoirs. *J. Volcanol. Geotherm. Res.* **2018**, *368*, 13–30. [CrossRef]
66. Thomas, R. Fluid evolution in relation to the emplacement of the Variscan granites in the Erzgebirge region: A review of the melt and fluid inclusion evidence. In *Metallogeny of Collisional Orogens*; Seltmann, R., Kämpf, H., Möller, P., Eds.; Czech Geological Survey: Prague, Czech Republic, 1994; pp. 70–81.
67. Thomas, R.; Förster, H.J.; Appel, K.; Webster, J. Formation of extremely F-rich hydrous melt fractions and hydrothermal fluids during differentiation of highly evolved tin-granite magmas: A melt/fluid-inclusion study. *Contrib. Miner. Pet.* **2005**, *148*, 582–601. [CrossRef]
68. Hoefs, J. *Stable Isotope Geochemistry*, 6th ed.; Springer: Berlin/Heidelberg, Germany, 2009. [CrossRef]
69. Morishita, Y.; Nishio, Y. Ore Genesis of the Takatori Tungsten–Quartz Vein Deposit, Japan: Chemical and Isotopic Evidence. *Minerals* **2021**, *11*, 765. [CrossRef]
70. Tornos, F.; Delgado, A.; Casquet, C.; Galindo, C. 300 Million years of episodic hydrothermal activity: Stable isotope evidence from hydrothermal rocks of the Eastern Iberian Central System. *Miner. Depos.* **2000**, *35*, 551–569. [CrossRef]
71. Moon, S.H.; Park, H.-I.; Ripley, E.M.; Lee, I. Mineralogic and stable isotope studies of cassiterite greisen mineralization in the Uljin area, Korea. *Econ. Geol.* **1996**, *91*, 916–933. [CrossRef]
72. Carruzzo, S.; Kontak, D.J.; Clarke, D.B.; Kyser, T.K. An integrated fluid-mineral stable-isotope study of the granite-hosted mineral deposits of the New Ross area, South Mountain Batholith, Nova Scotia, Canada: Evidence for multiple reservois. *Canad. Miner.* **2004**, *42*, 1425–1441. [CrossRef]
73. Myint, A.Z.; Yonezu, K.; Boyce, A.J.; Selby, D.; Scherstén, A.; Tindell, T.; Watanabe, K.; Swe, Y.M. Stable isotope and geochronological study of the Mawchi Sn-W deposit, Myanmar: Implications for timing of mineralization and ore genesis. *Ore Geol. Rev.* **2018**, *95*, 663–679. [CrossRef]

Disclaimer/Publisher's Note: The statements, opinions and data contained in all publications are solely those of the individual author(s) and contributor(s) and not of MDPI and/or the editor(s). MDPI and/or the editor(s) disclaim responsibility for any injury to people or property resulting from any ideas, methods, instructions or products referred to in the content.